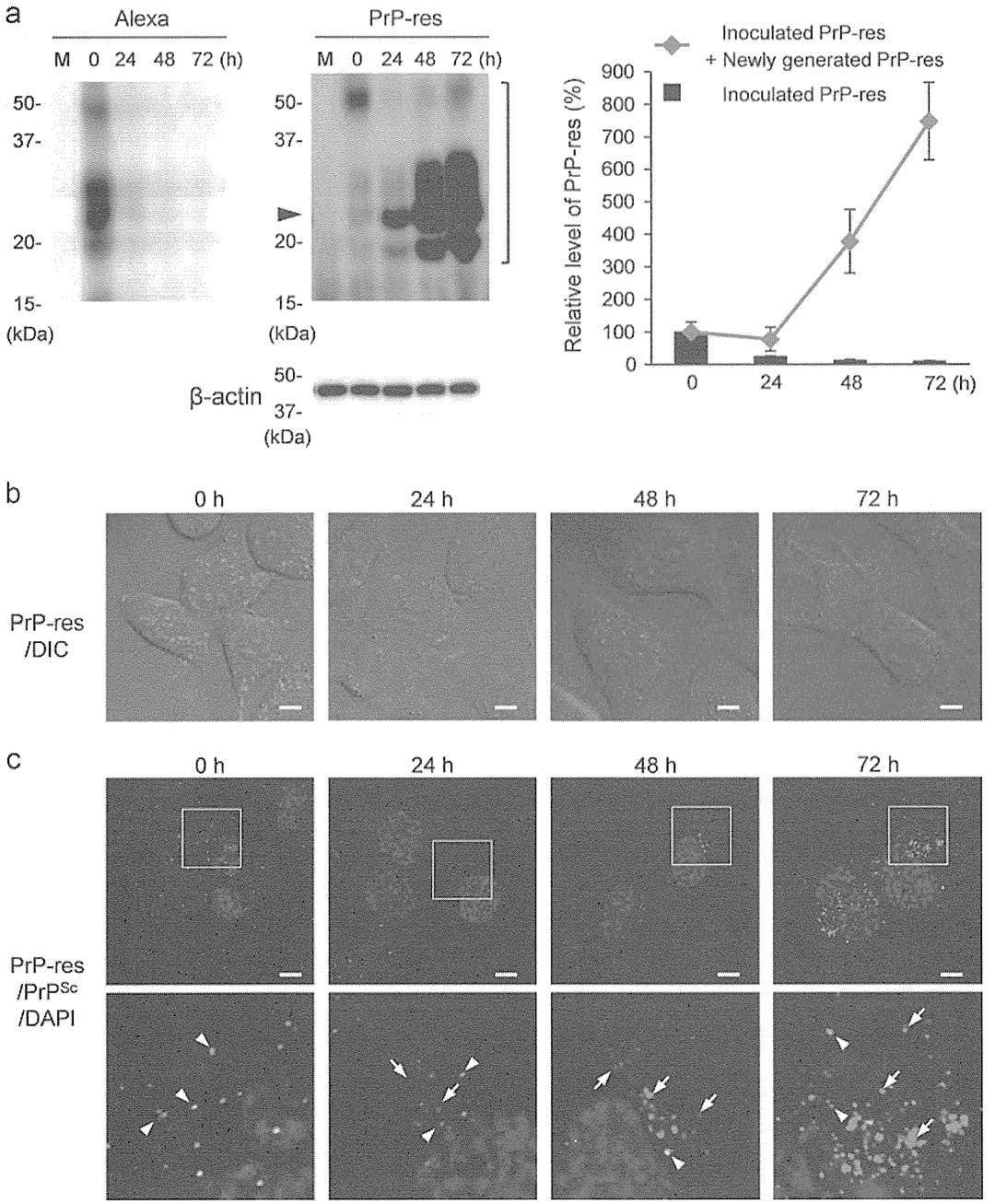

Fig. 4. Kinetics of inoculated PrP-res and *de novo* generation of PrP^{Sc}. (a) The levels of inoculated PrP-res and total PrP-res. N2a-3 cells grown on 12-well plates were inoculated with Af488-22-L-PrP-res. After the inoculation, the cells were cultured for the indicated period and then subjected to immunoblotting. As a control for detection of PrP-res, mock-infected cells were prepared (M). PK-untreated samples equivalent to 100 μg of total protein per lane were loaded to detect Af488-22-L-PrP-res with anti-Alexa Fluor 488 antibody (Alexa), while PK-digested samples equivalent to 100 μg of total protein were also loaded to monitor total PrP-res, which contained inoculated PrP-res and newly generated PrP-res with anti-PrP mAb 31C6 (PrP-res). β-actin was used as an internal control. Bands corresponding to monomeric and dimeric PrP^{Sc} (indicated by the square bracket) were quantified. The arrowhead indicates the mono-glycosylated form of PrP-res. The graph on the right shows the result of a quantitative analysis. Black bars indicate the inoculated PrP-res levels relative to that at 0 h and gray line indicates the total PrP-res levels relative to that at 0 h. Mean and SD of 3 independent experiments are shown. (b) Live-cell image of Af555-22-L-PrP-res. N2a-3 cells grown on chambered coverglass were inoculated with Af555-22-L-PrP-res and then cultured for the indicated time. Merged images containing Af555-22-L-PrP-res (red) and DIC are shown. (c) Discrimination of newly generated PrP^{Sc} from inoculated PrP-res in a single cell. The top panel shows the merged images of signals of Af555-22-L-PrP-res (red), PrP^{Sc} (green) and DAPI-stained nuclei (blue). The bottom panel shows the corresponding high-magnification images of the boxed region. Arrowheads indicate examples of inoculated PrP-res that was detected via both Alexa Fluor 555 (red, directly coupled to purified 22-L-PrP-res) and mAb 132 (green, indirect immuno-staining with Alexa Fluor 488-conjugated secondary antibody). As a result, inoculated PrP-res can be detected as yellow. Arrows indicate examples of newly generated PrP^{Sc} that was detected only with mAb 132 (green). Scale bar: 5 μm.

Influence of the impairment of intracellular transport on de novo generation of PrP^{Sc}

To determine which pathway of intracellular transport is involved in *de novo* generation of PrP^{Sc}, we analyzed the levels of newly generated PrP^{Sc} in cells in which trafficking between the endocytic compartments was selectively impaired by the overexpression of wild-type or dominant-negative mutants of Rab GTPase proteins (Fig. 7). The impairment of the endocytic-recycling pathway by overexpression of wild-type Rab22a or a dominant-negative mutant of Rab11a, which are known to affect the transport from early endosomes to recycling endosomes (Magadan et al., 2006) or the transport from recycling endosomes to plasma membrane (Ren et al., 1998), respectively, reduced the

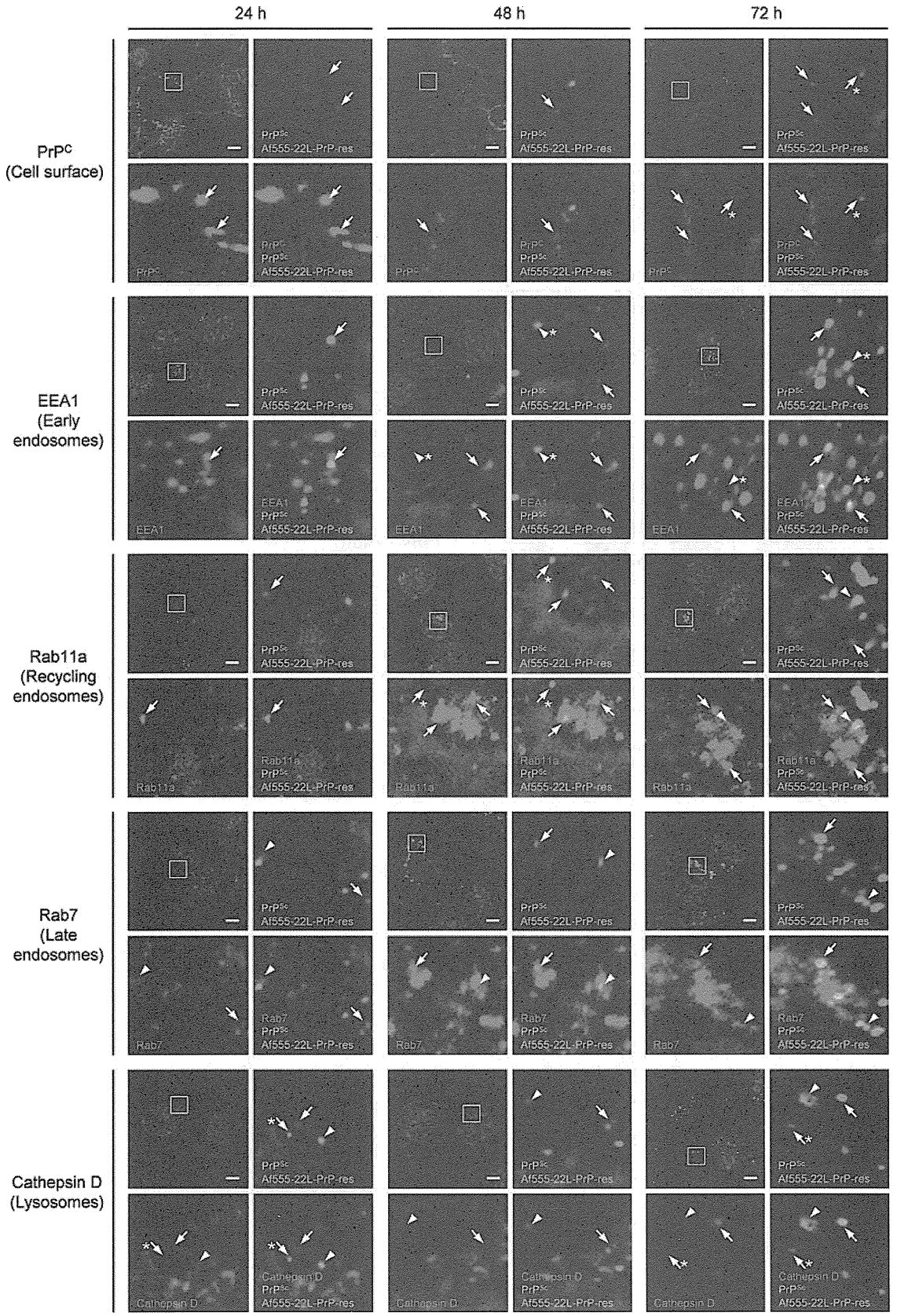

Fig. 5. Kinetics of the intracellular localization of inoculated PrP-res and newly generated PrP^{Sc}. N2a-3 cells inoculated with Af555-22-L-PrP-res were cultured for the indicated time and subjected to double-staining of PrP^{Sc} with mAb 132 and an organelle marker molecule as indicated. For staining of PrP^{C} at cell surface, cells were incubated with B103 antiserum prior to the fixation for PrP^{Sc}-specific detection. Alexa Fluor 647-conjugated secondary antibody was used to stain the marker molecules. The cell nuclei were counterstained with DAPI. The upper left image in each panel consists of four images shows a lower magnification view of a merged image of organelle marker molecule (red), PrP^{Sc} (green), Af555-22-L-PrP-res (cyan), and nuclei (blue). The other three images are the corresponding high-magnification image of the boxed region for the merged image of organelle marker and nuclei (bottom left), for the merged image of PrP^{Sc}, Af555-22-L-PrP-res and nuclei (upper right), and for the merged images of the organelle marker, PrP^{Sc}, Af555-22-L-PrP-res and nuclei (bottom right). Arrowheads indicate representative co-localization of Af555-22-L-PrP-res with organelle marker molecules, while arrows indicate that of newly generated PrP^{Sc} with organelle marker molecules. Arrowheads with asterisks indicate AF555-22-L-PrP-res that was not co-localized with organelle marker molecules, while arrows with asterisks indicate newly generated PrP^{Sc} that was not co-localized with organelle marker molecules. Co-localization areas were defined as pixels that were positive for both PrP^{Sc} and organelle marker signals, or that were positive for both Af555-22-L-PrP-res and organelle marker signals. Scale bars: 5 μm.

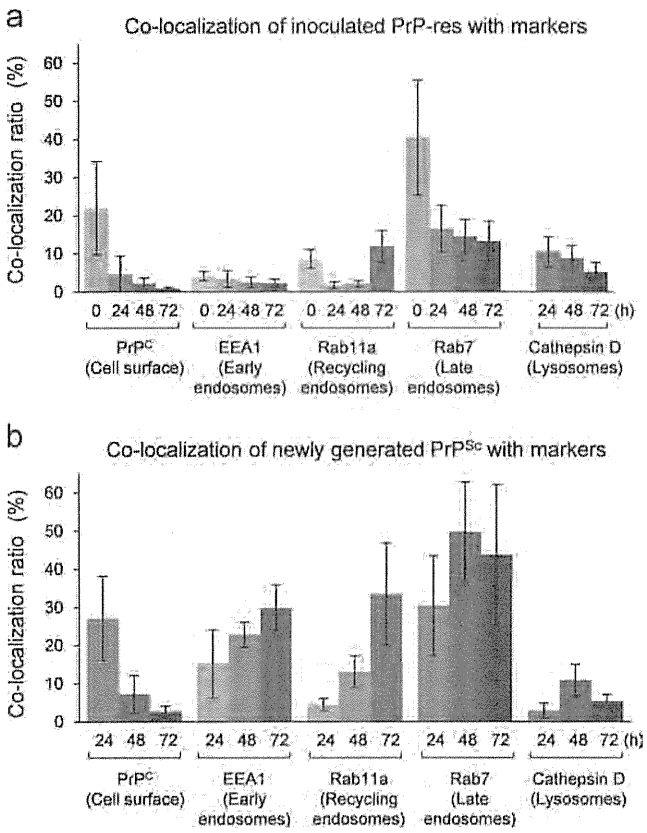

Fig. 6. Co-localization statistics. Co-localization analysis of the images shown in Fig. 5 was carried out as described in the Supplementary materials. (a) Ratio of the Af555-22-L-PrP-res signals co-localized with each marker to the sum of the Af555-22-L-PrP-res signals. (b) Ratio of the newly generated PrP^{Sc} signals co-localized with each marker to the sum of newly generated PrP^{Sc} signals. Mean and SD of the value acquired in 5 fields of view are shown. Total numbers of foci and cells used for co-localization statistics from the 5 view fields were listed in Table S5.

amount of *de novo* generated PrP^{Sc} at 48 hpi by 62% or 69% of the control (Fig. 7). Additionally, the impairment of the endo-lysosomal pathway by the overexpression of a dominant-negative mutant of Rab7, which is known to affect the transport from early endosomes to late endosomes and/or lysosomes (Bucci et al., 2000; Feng et al., 1995), also reduced the amount of *de novo* generated PrP^{Sc} at 48 hpi by 60% of the control (Fig. 7). A wild-type Rab9 is reported to be involved in the transport from late endosomes to TGN (Riederer et al., 1994). The overexpression of wild-type Rab9 reduced the amount of *de novo* generated PrP^{Sc} by 71% of the control; however, it was not clear which intracellular transport pathway was actually influenced (Fig. 7). The level of endogenous PrP^{C} in cells and cell-surface expression of PrP^{C} were not altered by overexpression of wild-type Rab9, wild-type Rab22a, a dominant-negative Rab7 mutant, or a dominant-negative Rab11a (Supplementary Fig. 1). Taken together, these results indicated that the inhibition of *de novo* generation of PrP^{Sc} was not caused by a change in the expression of PrP^{C}. These data suggested that intracellular transport along the endocytic-recycling pathway as well as the endo-lysosomal pathway is involved in the *de novo* generation of PrP^{Sc} after the inoculation of PrP-res.

Discussion

The lack of a method that can distinguish newly generated PrP^{Sc} from endogenous PrP^{C} and from inoculum-derived PrP^{Sc} was one of the obstacles to the investigation of the cellular events that mediate the *de novo* generation of PrP^{Sc} in the early stage of prion infection. Therefore, the analysis of intracellular dynamics of PrP^{Sc} just after inoculation of prions has been limited to inoculum-derived PrP^{Sc} as descried previously (Jen et al., 2010; Magalhaes et al., 2005). Here, we solved this problem with a combination of the fluorescent-dye-labeled purified PrP-res and PrP^{Sc}-specific staining with mAb 132. This technique allowed us to distinguish

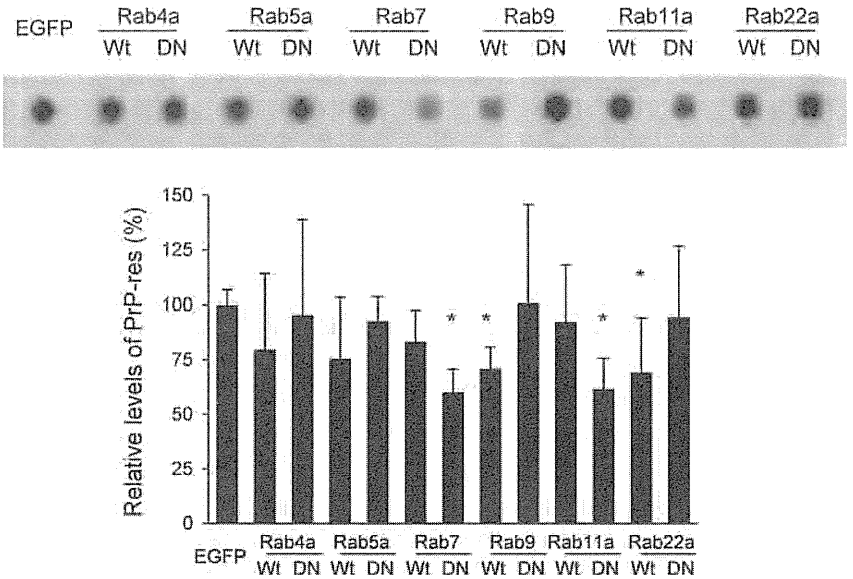

Fig. 7. Effect of overexpression of Rab GTPases on the *de novo* generation of PrP^{Sc}. N2a-3 cells grown in a 24-well plate were inoculated with unlabeled 22-L-PrP-res and were incubated for 6 h. After washing the cells, an expression plasmid encoding an EGFP-tagged wild-type (Wt) Rab GTPase, Rab4a, Rab5a, Rab7, Rab9, Rab11a or Rab22a, or an EGFP-tagged dominant-negative mutant (DN) of a Rab GTPases, Rab4aS22N (Roberts et al., 2001), Rab5aS34N (Stenmark et al., 1994), Rab7T22N (Feng et al., 1995), Rab9S21N (Riederer et al., 1994), Rab11aS25N (Ren et al., 1998) or Rab22aS19N (Weigert et al., 2004), was introduced. The expression vector pEGFP-C1 (Clontech) was used as a control. At 48 h after transfection, the cells were processed for dot-blotting to monitor PrP-res. A representative image of a dot-blot is shown on the top, and the graph below shows the levels of PrP-res relative to that of control plasmid-transfected cells (EGFP). Mean and SD of 4 independent experiments are depicted. Asterisks indicate a significant decrease compared to the control (Student's *t*-test, $p < 0.05$).

newly generated PrP^{Sc} from the inoculated PrP-res within individual cells.

Considering that the inoculated PrP-res was mainly detected in late endosomes and lysosomes (Figs. 5 and 6) and that its levels decreased from 24 to 72 h after the inoculation (Fig. 4), the PrP-res directed to the endo-lysosomal pathway appeared to be degraded in late endosomes and/or lysosomes. Previous studies showed that inoculated PrP-res is transported to late endosomes/lysosomes after being taken up by SN56 cells or primary sensory neurons (Jen et al., 2010; Magalhaes et al., 2005). Purified PrP-res of the Obihiro strain, which cannot establish a persistent infection in N2a-3 cells, was also transported to late endosomes and lysosomes; the intracellular distribution of Alexa Fluor-labeled Obihiro strain-derived PrP-res was indistinguishable from that of the 22-L strain-derived PrP-res and the inoculated PrP-res of Obihiro strain was degraded similarly to 22-L strain-derived PrP-res (data not shown). Amyloid fibrils of the Aβ1-42 peptide were also reported to be transported via the endo-lysosomal pathway in SN56 cells (Magalhaes et al., 2005). Taken together, the trafficking of PrP-res via the endo-lysosomal pathway appears to be a general pathway for degradation of exogenously introduced macromolecules, rather than a pathway specific to PrP^{Sc} and the propagation of prions (Saftig and Klumperman, 2009).

Recently, Goold et al. reported that the plasma membrane is one of the sites for conversion based on the results from experiments using PK-1 cells that express PrP^{C} tagged with Myc-epitope at the C-terminus (Goold et al., 2011). In this report, PrP^{Sc} was primarily generated at the plasma membrane within 2 min after prion challenge. Contrary to this report, we found no evidence that *de novo* generation of PrP^{Sc} primarily occurred at plasma membrane (Figs. 4–6). This discrepancy may be due to multiple factors, one of which includes clonal differences between these cell lines. For example, the former study showed that newly generated PrP^{Sc} attained steady levels by 2 h after inoculation of prions and approximately 20% of PK-1 cells in the cultures became PrP^{Sc}-positive. However, in the N2a-3 cells used in our study, the levels of newly generated PrP^{Sc} in the cells increased at least up to 72 hpi (Fig. 4), and most of the cells in the culture eventually became PrP^{Sc}-positive (data not shown). In addition, Goold et al. reported that PrP^{Sc} was detected at the cell membrane of prion-infected PK-1 cells; however, PrP^{Sc} was only weakly detected at the plasma membrane of N2a-3 cells persistently infected with prions, even when formic acid pre-treatment that was used for PrP^{Sc}-specific detection by Goold et al. was employed (data not shown). Finally, the differences between the two studies might be accounted for the different inocula (purified PrP-res vs. brain homogenate) used to initiate infection.

Most PrP^{C} is known to cycle between a peri-nuclear region of the cell and the plasma membrane via the endocytic-recycling pathway after being trafficked to the cell surface, but some portion of PrP^{C} is also delivered to late endosomes and lysosomes (Morris et al., 2006; Peters et al., 2003; Shyng et al., 1993). Considering that the newly generated PrP^{Sc} appeared in late endosomes, but was rarely observed in lysosomes at 24 hpi, at which time a large portion of the inoculated PrP-res was localized in late endosomes (Figs. 5 and 6), the initial conversion of PrP^{C} to PrP^{Sc} may occur in late endosomes, at least when purified PrP-res is used as an inoculum. This idea is consistent with the finding that overexpression of the dominant-negative mutant of Rab7, which inhibits transport from early endosomes to late endosomes and/or lysosomes (Bucci et al., 2000; Feng et al., 1995), partly inhibited the generation of PrP^{Sc} after the inoculation of PrP-res (reduced to 60% of the control, Fig. 7). This finding raises the possibility that although most of the inoculated PrP-res was transported to and degraded in late endosomes/lysosomes, smaller PrP-res oligomers might be generated in late endosomes during the degradation process. Such smaller PrP-res oligomers may initiate PrP^{C} conversion because smaller oligomers have greater seeding activity for the conversion of PrP^{C} and higher infectivity than larger PrP-res aggregates (Silveira et al., 2005).

Earlier studies suggested that in cells persistently infected with prions, PrP^{Sc} is formed either on the plasma membrane or during endocytic trafficking (Borchelt et al., 1992; Caughey and Raymond, 1991; Taraboulos et al., 1992). In later years, Béranger et al. and Marijanovic et al. reported that overexpression of dominant-negative mutants of Rab4a or Rab11a, which are known to impair the transport from early endosomes to the plasma membrane (Roberts et al., 2001) or from recycling endosomes to the plasma membrane (Ren et al., 1998), respectively, raised the PrP^{Sc} level (Beranger et al., 2002; Marijanovic et al., 2009). On the other hand, overexpression of wild-type Rab22a, which inhibits the transport from early endosomes to recycling endosomes (Magadan et al., 2006), reduced the PrP^{Sc} level in cells persistently infected with prions (Marijanovic et al., 2009). Based on these findings, one of the sites for PrP^{Sc} formation in cells persistently infected with prions is thought to be in the transport pathway from early endosomes to recycling endosomes. Also in the early stage of prion infection, we confirmed the inhibition of *de novo* generation of PrP^{Sc} by overexpression of a wild-type Rab22a (reduced to 69% of the control, Fig. 7), consistent with the results of Marijanovic et al. in persistently prion-infected cells (Marijanovic et al., 2009). However, unlike the findings in cells persistently infected with prions, the generation of PrP^{Sc} after the inoculation of PrP-res was partly inhibited by overexpression of a dominant-negative Rab11a mutant (reduced to 62% of the control, Fig. 7). These observations suggested that the initiation of PrP^{Sc} generation shortly after PrP-res inoculation required the recycling pathway between recycling endosomes and the plasma membrane. Further studies will be required to explain the apparent inconsistency between these results. However, the newly generated PrP^{Sc} appeared at the plasma membrane and in early endosomes where the inoculated PrP-res was rarely detected at 24 hpi (Figs. 5 and 6), suggesting the involvement of the recycling pathway; therefore, either the exogenous PrP-res degraded to an undetectable level or PrP^{Sc} newly generated in late endosomes was recycled back to the plasma membrane and acted as a "seed" for conversion. Moreover, the marked increase in the newly generated PrP^{Sc} at early and recycling endosomes during the following 48 h (Figs. 5 and 6) suggested that efficient generation of PrP^{Sc} occurred once the PrP^{Sc} was transferred to the endocytic-recycling pathway.

The results in this study suggest that the transfer of the inoculated PrP-res and/or newly generated PrP^{Sc} from the endo-lysosomal pathway to the endocytic-recycling pathway is important for efficient PrP^{Sc} formation after prion inoculation. One possible route of such transfer is the trafficking from the late endosomes to the plasma membrane through the TGN, a route by which cation-independent mannose-6-phosphate receptor (CIMPR) is transported (Maxfield and McGraw, 2004). CIMPR delivers hydrolase precursors from the Golgi apparatus to the endosomes and releases hydrolases into compartments in the process of late endosome formation; CIMPR is then recycled back from late endosomes to the TGN by retrograde transport. CIMPR in the TGN is also delivered to the plasma membrane (Ghosh et al., 2003). The overexpression of Rab9, which is involved in this retrograde transport of CIMPR (Riederer et al., 1994), was reported to decrease the levels of PrP^{Sc} in cells persistently infected with prions (Gilch et al., 2009) as well as inhibit the generation of PrP^{Sc} after prion inoculation (this study), suggesting that the trafficking from late endosomes to the TGN may be involved in the generation of PrP^{Sc}.

Direct transport from late endosomes to the plasma membrane might be an alternative route. This atypical transport was reported

in the trafficking of class II molecules of the major histocompatibility complex (MHC) and CD1 family molecules in antigen-presenting cells (Gelin et al., 2009; Neefjes et al., 2011). Furthermore, MHC class II molecules are also known to be transported in the process of exosomes release (Berger and Roche, 2009; Von Bartheld and Altick, 2011). Considering the fact that PrP^{C} is present on the membranes of both multivesicular bodies and intraluminal vesicles and that PrP^{Sc} as well as PrP^{C} are released from cells with exosomes (Fevrier et al., 2004), the inoculated PrP-res and/or newly generated PrP^{Sc} in late endosomes may be recycled back to the plasma membrane through multivesicular bodies via a pathway similar to the MHC class II molecules. This idea is consistent with the finding that *de novo* generation of PrP^{Sc} was inhibited by the overexpression of the dominant-negative Rab11a mutant, which also inhibits the release of exosomes (Savina et al., 2002). The PrP^{Sc} recycled to the plasma membrane via these mechanisms may, in turn, contribute to *de novo* generation of PrP^{Sc} in the compartments on the endocytic-recycling pathway.

The intracellular dynamics of PrP^{Sc} in CNS neurons in the early stages after prion infection is largely unknown. It was reported that PrP^{Sc} could be detected in endosomal and lysosomal fractions prior to the detection of PrP^{Sc} in the plasma membrane fraction after intracerebral inoculation of prions (Dearmond and Bajsarowicz, 2010), and that protease-sensitive PrP^{Sc} could be detected in early and recycling endosomes in neurons in the hippocampus during the preclinical stage of infected mice (Godsave et al., 2008). These facts suggest that there are similarities in prion propagation in neuroblastoma cells and neurons in CNS.

In this study, we showed the intracellular dynamics of inoculated PrP-res in prion-susceptible neuroblastoma cells. Our data suggest that transfer of inoculated PrP-res from the endo-lysosomal pathway to the endocytic-recycling pathway is involved in the initiation of efficient *de novo* generation of PrP^{Sc} in the early stage of infection (Fig. 8). However, further analyses are required for understanding the mechanisms of prion propagation in neurons in CNS. Experiments are underway to clarify the intracellular site for PrP^{Sc} generation in neurons in CNS using PrP^{Sc}-specific staining with mAb 132.

Materials and methods

Antibodies, expression plasmids, and reagents

Anti-PrP mouse mAbs 31C6 and 132 and a rabbit polyclonal antibody B103 were used (Horiuchi et al., 1995; Kim et al., 2004). The other commercially available primary and secondary antibodies that were used for immunoblotting and IFA are listed in Table S1. Alexa Fluor 488- and 555-conjugated Tfn and Alexa Fluor 488-conjugated LDL (Life Technologies) were used as markers for the endocytic pathway. Expression plasmids encoding EGFP-tagged Rab GTPases were prepared as described in Supplemental materials according to methods described elsewhere (Table S2 and S3) (Fukuda, 2003).

Cell culture

N2a-3 cells, a subclone of the mouse neuroblastoma cell line Neuro2a, were cultured as described previously (Uryu et al., 2007).

Purification of PrP-res

PrP-res was prepared from detergent-resistant membranes as described previously (Baron et al., 2011) with slight modifications (Supplementary materials). The purification procedure included a PK treatment, so from this point forward we use the term "PrP-res" to indicate the purified, PK-treated PrP^{Sc}.

Fluorescent-dye-labeling of PrP-res

PrP-res in PBS (10 μg in 50 μl) containing 0.5% Zwittergent 3-14 was sonicated with a Cross Ultrasonic Protein Auto Activating Instrument, ELSTEIN NP070-GOT (Nepa Gene), by 4 cycles of

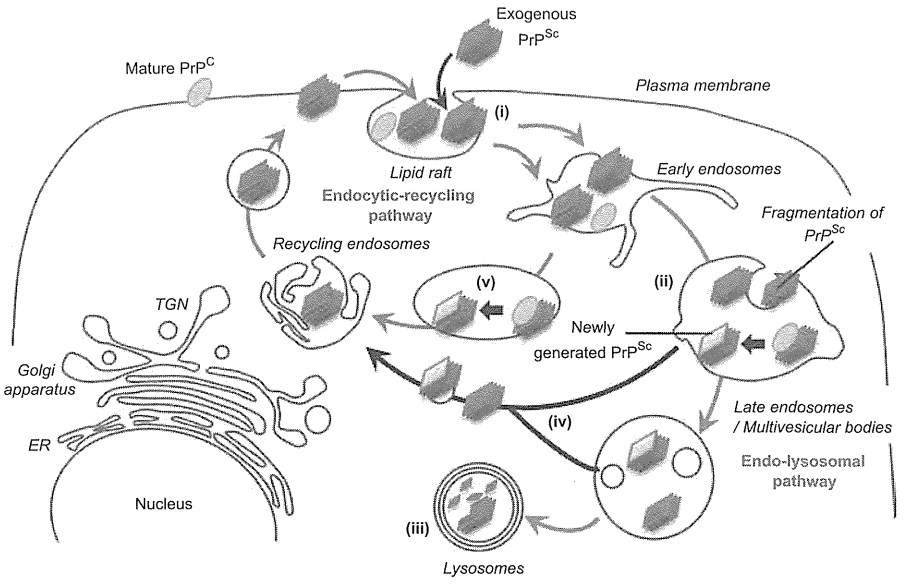

Fig. 8. Summary of intracellular dynamics of inoculated PrP^{Sc} and *de novo* generation of PrP^{Sc} in early stage of prion infection. Exogenously introduced PrP^{Sc} (red parallelograms) is internalized into a cell (i). Although inoculated PrP^{Sc} is transported throughout endocytic compartment immediately after internalization, most of the inoculated PrP^{Sc} eventually directed to endo-lysosomal pathway (indicated as red arrows) and is delivered to lysosomes and degraded (iii). Conversion of PrP^{C} (pink ellipse) to PrP^{Sc} (pink parallelogram) may be initiated by fragmented inoculated PrP^{Sc} (a smaller PrP^{Sc} oligomer) that is generated during the transport on the endo-lysosomal pathway (ii). A smaller PrP^{Sc} oligomer generated by fragmentation of inoculated PrP^{Sc} and/or newly generated PrP^{Sc} is transferred from the endo-lysosomal pathway to the endocytic-recycling pathway (iv). Once PrP^{Sc} that is capable of inducing conversion (blue parallelograms) is transferred to endocytic-recycling pathway (indicated as blue arrows) initiates efficient PrP^{Sc} formation that leads to the establishment of prion infection. The sites where efficient conversion occurs are thought to be early endosomes and recycling endosomes (v).

15 min-sonication followed by 5 min-incubation at 4 °C prior to fluorescent-dye labeling. The PrP-res was then mixed with 200 μg of Alexa Fluor 488 succinimidyl ester or Alexa Fluor 555 succinimidyl ester (Life Technologies) dissolved in 5 μl of anhydrous dimethyl sulfoxide (Sigma). Fluorescent-dye labeling was performed under 16 cycles of 15 min-sonication followed by 30 min-incubation at 4 °C. To quench the excess reactive dye, 3 ml of 50 mM glycine in PBS was mixed with the PrP-res and the sample was centrifuged at 45,000 rpm for 30 min at 4 °C in a S80AT3 rotor (Hitachi). The pellet was washed twice with 50 mM glycine in PBS and each wash was followed by centrifugation; the final pellet was resuspended in 100 μl of PBS with sonication. The fluorescent-dye-labeled PrP-res or unlabeled PrP-res was subjected to SDS-PAGE followed by fluorescent imaging with Typhoon FLA 9000 (GE Healthcare) or by silver-staining with 2D-SILVER STAIN-II (Cosmo bio CO.), respectively.

Inoculation of PrP-res

Purified PrP-res or fluorescent-dye-labeled PrP-res was diluted with Opti-MEM (Life technologies), sonicated with an ELSTEIN NP070-GOT sonicator for 5 min, and centrifuged at 10,000 × *g* for 10 min to remove large PrP-res aggregates. The supernatant was diluted with Opti-MEM at 10 ng PrP-res/200 μl or 20 ng PrP-res/250 μl or 35 ng PrP-res/500 μl for use on 8-well Lab-Tek II chambered coverglass (Thermo Scientific) or 24- or 12-well plates, respectively. The culture medium for the N2a-3 cells grown on a chambered coverglass or in the multi-well plates was replaced with Opti-MEM containing PrP-res, and the cells were then incubated for 2 or 6 h at 37 °C. After incubation, the cells were washed three times with pre-warmed PBS and then cultured in Opti-MEM containing 10% fetal bovine serum (FBS), 1% non-essential amino acids (NEAA; Gibco), and 1X penicillin-streptomycin solution (100 U/ml–100 μg/ml, PS; Gibco).

Immunofluorescence assay (IFA)

IFA, including PrP^{Sc}-specific staining, was carried out as described previously (Yamasaki et al., 2012) with some modifications. Cells were grown on an 8-well Lab-Tek II chambered coverglass and all the staining procedures were carried out without the removal of the media chamber. For double staining of cell surface PrP^{C} and PrP^{Sc}, living cells were incubated with B103 (5 μg/ml) in Opti-MEM for 15 min at 37 °C. The cells were then immediately fixed with pre-warmed 4% paraformaldehyde with 4% sucrose in PBS for 10 min and blocked with 5% FBS in PBS. Cells were then incubated with secondary antibody, and the cells were fixed again with 4% paraformaldehyde in PBS for 10 min and were subjected to the PrP^{Sc}-specific staining. To counterstain cell nuclei, cells were incubated with 5 μg/ml of 4', 6-diamidino-2-phenylindole, dilactate (DAPI; Invitrogen) in PBS at room temperature (rt) for 30 min. Finally, the media chamber was filled with PBS and confocal fluorescent images were acquired with a 63 × objective lens on a Zeiss LSM700 inverted microscope and the ZEN 2009 software. Z-series of the images were taken at every 0.8 μm steps from the top to bottom of the cells in the area.

Transfection

N2a-3 cells seeded onto 8-well chambered coverglass or 24-well plates at 1:5 ratio were cultured in Dulbecco's modified Eagle's medium (DMEM; ICN Biomedicals) for 2 days prior to the inoculation of PrP-res and transfection. The cells were transfected with 2.8% Lipofectamine 2000 (Invitrogen) and 2 μg/ml expression plasmid in 250 μl (8-well chamber) or 500 μl (24-well plate) of Opti-MEM that contained 8% FBS, 0.8% NEAA, and 0.8X PS. After transfection (24 h), the medium was replaced with fresh Opti-MEM containing 10% FBS, 1% NEAA and 1X PS and cultured until used for immunoblots or IFA.

Immunoblotting and dot-blotting

Immunoblotting and dot-blotting were performed to monitor PrP and other molecules as described elsewhere (Nakamitsu et al., 2010; Uryu et al., 2007). To monitor PrP-res via immunoblotting, the protein concentration of cell lysate was adjusted to 1 mg/ml and the samples were then treated with 1 μg/ml of PK for 20 min at 37 °C. Meanwhile, to monitor Alexa Fluor 488-labeled PrP-res, PK treatment was omitted. The cell lysates were incubated with 50 μg/ml of DNase I (Roche) for 15 min at rt. Proteins were concentrated by incubating the samples with 0.3% phosphotungstic acid for 20 min at rt; this incubation was followed by centrifugation at 20,500*g* for 20 min at 4 °C.

To monitor PrP-res via dot-blotting, cell lysate equivalent to 40 μg of total protein per well was transferred onto a polyvinylidene difluoride (PVDF) membrane by a dot-blotter (Bio-Rad). The PVDF membrane was treated with 20 μg/ml of PK for 1 h at 37 °C and then incubated with 1 mM Pefabloc SC for 15 min at 4 °C. The membrane was treated with 50 μg/ml of DNase I for 15 min at rt and then incubated in 3 M GdnSCN for 30 min at rt. Samples on each membrane were then subjected to immuno-detection with mAb 31C6 and HRP-conjugated secondary antibody. ECL Western Blotting Detection Reagents (GE Healthcare) and a LAS-3000 chemiluminescence image analyzer (Fuji Film) were used to visualize the immunoreactive proteins.

Acknowledgments

T.Y. is supported by a Grant-in-Aid for JSPS Fellows (No. 22 · 4181). This work was supported by a Grant-in-Aid for Science Research (A) (Grant no. 23248050), a Grant from the Global COE Program (F-001) and the Program for Leading Graduate Schools (F01), and the Japan Initiative for Global Research Network on Infectious Diseases (J-GRID), from the Ministry of Education, Culture, Sports, Science, and Technology, Japan. This work was also supported by grants for TSE research (H23-Shokuhin-Ippan-005) and Research on Measures for Intractable Diseases from the Ministry of Health, Labour and Welfare of Japan and in part by the Intramural Research Program, National Institute of Allergy and Infectious Diseases, National Institutes of Health. We also thank Zensho Co. Ltd. for BSL3 facility.

Appendix A. Supporting information

Supplementary data associated with this article can be found in the online version at http://dx.doi.org/10.1016/j.virol.2013.11.007.

References

Baron, G.S., Hughson, A.G., Raymond, G.J., Offerdahl, D.K., Barton, K.A., Raymond, L.D., Dorward, D.W., Caughey, B., 2011. Effect of glycans and the glycophosphatidylinositol anchor on strain dependent conformations of scrapie prion protein: improved purifications and infrared spectra. Biochemistry 50, 4479–4490.

Beranger, F., Mange, A., Goud, B., Lehmann, S., 2002. Stimulation of PrP (C) retrograde transport toward the endoplasmic reticulum increases accumulation of PrP(Sc) in prion-infected cells. J. Biol. Chem. 277, 38972–38977.

Berger, A.C., Roche, P.A., 2009. MHC class II transport at a glance. J. Cell Sci. 122, 1–4.

Borchelt, D.R., Taraboulos, A., Prusiner, S.B., 1992. Evidence for synthesis of scrapie prion proteins in the endocytic pathway. J. Biol. Chem. 267, 16188–16199.

Bucci, C., Thomsen, P., Nicoziani, P., McCarthy, J., van Deurs, B., 2000. Rab7: a key to lysosome biogenesis. Mol. Biol. Cell 11, 467–480.

Caughey, B., Raymond, G.J., 1991. The scrapie-associated form of PrP is made from a cell surface precursor that is both protease- and phospholipase-sensitive. J. Biol. Chem. 266, 18217–18223.
Dearmond, S.J., Bajsarowicz, K., 2010. PrPSc accumulation in neuronal plasma membranes links Notch-1 activation to dendritic degeneration in prion diseases. Mol. Neurodegener 5, 6.
Feng, Y., Press, B., Wandinger-Ness, A., 1995. Rab 7: an important regulator of late endocytic membrane traffic. J. Cell Biol. 131, 1435–1452.
Fevrier, B., Vilette, D., Archer, F., Loew, D., Faigle, W., Vidal, M., Laude, H., Raposo, G., 2004. Cells release prions in association with exosomes. Proc. Natl. Acad. Sci. U.S.A 101, 9683–9688.
Fukuda, M., 2003. Distinct Rab binding specificity of Rim1, Rim2, rabphilin, and Noc2. Identification of a critical determinant of Rab3A/Rab27A recognition by Rim2. J. Biol. Chem. 278, 15373–15380.
Gauczynski, S., Nikles, D., El-Gogo, S., Papy-Garcia, D., Rey, C., Alban, S., Barritault, D., Lasmezas, C.I., Weiss, S., 2006. The 37-kDa/67-kDa laminin receptor acts as a receptor for infectious prions and is inhibited by polysulfated glycanes. J. Infect. Dis. 194, 702–709.
Gelin, C., Sloma, I., Charron, D., Mooney, N., 2009. Regulation of MHC II and CD1 antigen presentation: from ubiquity to security. J. Leukoc. Biol. 85, 215–224.
Ghosh, P., Dahms, N.M., Kornfeld, S., 2003. Mannose 6-phosphate receptors: new twists in the tale. Nat. Rev. Mol. Cell Biol. 4, 202–212.
Gilch, S., Bach, C., Lutzny, G., Vorberg, I., Schatzl, H.M., 2009. Inhibition of cholesterol recycling impairs cellular PrP(Sc) propagation. Cell. Mol. Life Sci. 66, 3979–3991.
Godsave, S.F., Wille, H., Kujala, P., Latawiec, D., DeArmond, S.J., Serban, A., Prusiner, S.B., Peters, P.J., 2008. Cryo-immunogold electron microscopy for prions: toward identification of a conversion site. J. Neurosci. 28, 12489–12499.
Goold, R., Rabbanian, S., Sutton, L., Andre, R., Arora, P., Moonga, J., Clarke, A.R., Schiavo, G., Jat, P., Collinge, J., Tabrizi, S.J., 2011. Rapid cell-surface prion protein conversion revealed using a novel cell system. Nat. Commun. 2, 281.
Greil, C.S., Vorberg, I.M., Ward, A.E., Meade-White, K.D., Harris, D.A., Priola, S.A., 2008. Acute cellular uptake of abnormal prion protein is cell type and scrapie-strain independent. Virology 379, 284–293.
Hijazi, N., Kariv-Inbal, Z., Gasset, M., Gabizon, R., 2005. PrPSc incorporation to cells requires endogenous glycosaminoglycan expression. J. Biol. Chem. 280, 17057–17061.
Horiuchi, M., Yamazaki, N., Ikeda, T., Ishiguro, N., Shinagawa, M., 1995. A cellular form of prion protein (PrPC) exists in many non-neuronal tissues of sheep. J. Gen. Virol. 76 (Pt 10), 2583–2587.
Horonchik, L., Tzaban, S., Ben-Zaken, O., Yedidia, Y., Rouvinski, A., Papy-Garcia, D., Barritault, D., Vlodavsky, I., Taraboulos, A., 2005. Heparan sulfate is a cellular receptor for purified infectious prions. J. Biol. Chem. 280, 17062–17067.
Ikonen, E., 2008. Cellular cholesterol trafficking and compartmentalization. Nat. Rev. Mol. Cell Biol. 9, 125–138.
Jen, A., Parkyn, C.J., Mootoosamy, R.C., Ford, M.J., Warley, A., Liu, Q., Bu, G., Baskakov, I.V., Moestrup, S., McGuinness, L., Emptage, N., Morris, R.J., 2010. Neuronal low-density lipoprotein receptor-related protein 1 binds and endocytoses prion fibrils via receptor cluster 4. J. Cell Sci. 123, 246–255.
Kim, C.L., Umetani, A., Matsui, T., Ishiguro, N., Shinagawa, M., Horiuchi, M., 2004. Antigenic characterization of an abnormal isoform of prion protein using a new diverse panel of monoclonal antibodies. Virology 320, 40–51.
Magadan, J.G., Barbieri, M.A., Mesa, R., Stahl, P.D., Mayorga, L.S., 2006. Rab22a regulates the sorting of transferrin to recycling endosomes. Mol. Cell. Biol. 26, 2595–2614.
Magalhaes, A.C., Baron, G.S., Lee, K.S., Steele-Mortimer, O., Dorward, D., Prado, M.A., Caughey, B., 2005. Uptake and neuritic transport of scrapie prion protein coincident with infection of neuronal cells. J. Neurosci. 25, 5207–5216.
Marijanovic, Z., Caputo, A., Campana, V., Zurzolo, C., 2009. Identification of an intracellular site of prion conversion. PLoS Pathog. 5, e1000426.
Maxfield, F.R., McGraw, T.E., 2004. Endocytic recycling. Nat. Rev. Mol. Cell Biol. 5, 121–132.
McKinley, M.P., Taraboulos, A., Kenaga, L., Serban, D., Stieber, A., DeArmond, S.J., Prusiner, S.B., Gonatas, N., 1991. Ultrastructural localization of scrapie prion proteins in cytoplasmic vesicles of infected cultured cells. Lab. Invest. 65, 622–630.
Morris, R.J., Parkyn, C.J., Jen, A., 2006. Traffic of prion protein between different compartments on the neuronal surface, and the propagation of prion disease. FEBS Lett. 580, 5565–5571.
Nakamitsu, S., Kurokawa, A., Yamasaki, T., Uryu, M., Hasebe, R., Horiuchi, M., 2010. Cell density-dependent increase in the level of protease-resistant prion protein in prion-infected Neuro2a mouse neuroblastoma cells. J. Gen. Virol. 91, 563–569.
Neefjes, J., Jongsma, M.L., Paul, P., Bakke, O., 2011. Towards a systems understanding of MHC class I and MHC class II antigen presentation. Nat. Rev. Immunol. 11, 823–836.
Paquet, S., Daude, N., Courageot, M.P., Chapuis, J., Laude, H., Vilette, D., 2007. PrPc does not mediate internalization of PrPSc but is required at an early stage for de novo prion infection of Rov cells. J. Virol. 81, 10786–10791.
Peters, P.J., Mironov Jr., A., Peretz, D., van Donselaar, E., Leclerc, E., Erpel, S., DeArmond, S.J., Burton, D.R., Williamson, R.A., Vey, M., Prusiner, S.B., 2003. Trafficking of prion proteins through a caveolae-mediated endosomal pathway. J. Cell Biol. 162, 703–717.
Pimpinelli, F., Lehmann, S., Maridonneau-Parini, I., 2005. The scrapie prion protein is present in flotillin-1-positive vesicles in central- but not peripheral-derived neuronal cell lines 21, 2063–2072Eur. J. Neurosci. 21, 2063–2072.
Prusiner, S.B., 1998. Prions. Proc. Natl. Acad. Sci. U.S.A 95, 13363–13383.
Ren, M., Xu, G., Zeng, J., De Lemos-Chiarandini, C., Adesnik, M., Sabatini, D.D., 1998. Hydrolysis of GTP on rab11 is required for the direct delivery of transferrin from the pericentriolar recycling compartment to the cell surface but not from sorting endosomes. Proc. Natl. Acad. Sci. U.S.A 95, 6187–6192.
Riederer, M.A., Soldati, T., Shapiro, A.D., Lin, J., Pfeffer, S.R., 1994. Lysosome biogenesis requires Rab9 function and receptor recycling from endosomes to the trans-Golgi network. J. Cell Biol. 125, 573–582.
Roberts, M., Barry, S., Woods, A., van der Sluijs, P., Norman, J., 2001. PDGF-regulated rab4-dependent recycling of alphavbeta3 integrin from early endosomes is necessary for cell adhesion and spreading. Curr. Biol. 11, 1392–1402.
Saftig, P., Klumperman, J., 2009. Lysosome biogenesis and lysosomal membrane proteins: trafficking meets function. Nat. Rev. Mol. Cell Biol. 10, 623–635.
Savina, A., Vidal, M., Colombo, M.I., 2002. The exosome pathway in K562 cells is regulated by Rab11. J. Cell Sci. 115, 2505–2515.
Shyng, S.L., Huber, M.T., Harris, D.A., 1993. A prion protein cycles between the cell surface and an endocytic compartment in cultured neuroblastoma cells. J. Biol. Chem. 268, 15922–15928.
Silveira, J.R., Raymond, G.J., Hughson, A.G., Race, R.E., Sim, V.L., Hayes, S.F., Caughey, B., 2005. The most infectious prion protein particles. Nature 437, 257–261.
Stenmark, H., 2009. Rab GTPases as coordinators of vesicle traffic. Nat. Rev. Mol. Cell Biol. 10, 513–525.
Stenmark, H., Parton, R.G., Steele-Mortimer, O., Lutcke, A., Gruenberg, J., Zerial, M., 1994. Inhibition of rab5 GTPase activity stimulates membrane fusion in endocytosis. EMBO J. 13, 1287–1296.
Taraboulos, A., Raeber, A.J., Borchelt, D.R., Serban, D., Prusiner, S.B., 1992. Synthesis and trafficking of prion proteins in cultured cells. Mol. Biol. Cell 3, 851–863.
Taraboulos, A., Serban, D., Prusiner, S.B., 1990. Scrapie prion proteins accumulate in the cytoplasm of persistently infected cultured cells. J. Cell Biol. 110, 2117–2132.
Uryu, M., Karino, A., Kamihara, Y., Horiuchi, M., 2007. Characterization of prion susceptibility in Neuro2a mouse neuroblastoma cell subclones. Microbiol. Immunol. 51, 661–669.
Veith, N.M., Plattner, H., Stuermer, C.A., Schulz-Schaeffer, W.J., Burkle, A., 2009. Immunolocalisation of PrPSc in scrapie-infected N2a mouse neuroblastoma cells by light and electron microscopy. Eur. J. Cell Biol. 88, 45–63.
Vey, M., Pilkuhn, S., Wille, H., Nixon, R., DeArmond, S.J., Smart, E.J., Anderson, R.G., Taraboulos, A., Prusiner, S.B., 1996. Subcellular colocalization of the cellular and scrapie prion proteins in caveolae-like membranous domains. Proc. Natl. Acad. Sci. U.S.A 93, 14945–14949.
Von Bartheld, C.S., Altick, A.L., 2011. Multivesicular bodies in neurons: distribution, protein content, and trafficking functions. Prog. Neurobiol. 93, 313–340.
Vorberg, I., Raines, A., Priola, S.A., 2004. Acute formation of protease-resistant prion protein does not always lead to persistent scrapie infection in vitro. J. Biol. Chem. 279, 29218–29225.
Wang, F., Wang, X., Yuan, C.G., Ma, J., 2010. Generating a prion with bacterially expressed recombinant prion protein. Science 327, 1132–1135.
Weigert, R., Yeung, A.C., Li, J., Donaldson, J.G., 2004. Rab22a regulates the recycling of membrane proteins internalized independently of clathrin. Mol. Biol. Cell 15, 3758–3770.
Yamasaki, T., Suzuki, A., Shimizu, T., Watarai, M., Hasebe, R., Horiuchi, M., 2012. Characterization of intracellular localization of PrP(Sc) in prion-infected cells using a mAb that recognizes the region consisting of aa 119–127 of mouse PrP. J. Gen. Virol. 93, 668–680.

Journal of Virology

Conformational Properties of Prion Strains Can Be Transmitted to Recombinant Prion Protein Fibrils in Real-Time Quaking-Induced Conversion

Kazunori Sano, Ryuichiro Atarashi, Daisuke Ishibashi, Takehiro Nakagaki, Katsuya Satoh and Noriyuki Nishida

J. Virol. **2014, 88(20):11791. DOI: 10.1128/JVI.00585-14. Published Ahead of Print 30 July 2014.**

JVI Journals ASM.org

Conformational Properties of Prion Strains Can Be Transmitted to Recombinant Prion Protein Fibrils in Real-Time Quaking-Induced Conversion

Kazunori Sano,[a] Ryuichiro Atarashi,[a,b] Daisuke Ishibashi,[a] Takehiro Nakagaki,[a] Katsuya Satoh,[a] Noriyuki Nishida[a]

Department of Molecular Microbiology and Immunology, Nagasaki University Graduate School of Biomedical Sciences, Nagasaki, Japan[a]; Research Centre for Genomic Instability and Carcinogenesis, Nagasaki University, Nagasaki, Japan[b]

ABSTRACT

The phenomenon of prion strains with distinct biological characteristics has been hypothesized to be involved in the structural diversity of abnormal prion protein (PrP^{Sc}). However, the molecular basis of the transmission of strain properties remains poorly understood. Real-time quaking-induced conversion (RT-QUIC) is a cell-free system that uses *Escherichia coli*-derived recombinant PrP (rPrP) for the sensitive detection of PrP^{Sc}. To investigate whether the properties of various prion strains can be transmitted to amyloid fibrils consisting of rPrP (rPrP fibrils) using RT-QUIC, we examined the secondary structure, conformational stability, and infectivity of rPrP fibrils seeded with PrP^{Sc} derived from either the Chandler or the 22L strain. In the first round of the reaction, there were differences in the secondary structures, especially in bands attributed to β-sheets, as determined by infrared spectroscopy, and conformational stability between Chandler-seeded (1st-rPrP-fib^{Ch}) and 22L-seeded (1st-rPrP-fib^{22L}) rPrP fibrils. Of note, specific identifying characteristics of the two rPrP fibril types seen in the β-sheets resembled those of the original PrP^{Sc}. Furthermore, the conformational stability of 1st-rPrP-fib^{Ch} was significantly higher than that of 1st-rPrP-fib^{22L}, as with Chandler and 22L PrP^{Sc}. The survival periods of mice inoculated with 1st-rPrP-fib^{Ch} or 1st-rPrP-fib^{22L} were significantly shorter than those of mice inoculated with mixtures from the mock 1st-round RT-QUIC procedure. In contrast, these biochemical characteristics were no longer evident in subsequent rounds, suggesting that nonspecific uninfected rPrP fibrils became predominant probably because of their high growth rate. Together, these findings show that at least some strain-specific conformational properties can be transmitted to rPrP fibrils and unknown cofactors or environmental conditions may be required for further conservation.

IMPORTANCE

The phenomenon of prion strains with distinct biological characteristics is assumed to result from the conformational variations in the abnormal prion protein (PrP^{Sc}). However, important questions remain about the mechanistic relationship between the conformational differences and the strain diversity, including how strain-specific conformations are transmitted. In this study, we investigated whether the properties of diverse prion strains can be transmitted to amyloid fibrils consisting of *E. coli*-derived recombinant PrP (rPrP) generated by real-time quaking-induced conversion (RT-QUIC), a recently developed *in vitro* PrP^{Sc} formation method. We demonstrate that at least some of the strain-specific conformational properties can be transmitted to rPrP fibrils in the first round of RT-QUIC by examining the secondary structure, conformational stability, and infectivity of rPrP fibrils seeded with PrP^{Sc} derived from either the Chandler or the 22L prion strain. We believe that these findings will advance our understanding of the conformational basis underlying prion strain diversity.

Prion diseases, or transmissible spongiform encephalopathies (TSEs), are infectious and fatal neurodegenerative disorders characterized by progressive spongiform changes and the accumulation of abnormal prion protein (PrP^{Sc}) in the central nervous system. Although the pathogenic mechanisms have not been fully elucidated, prion disease is thought to occur through autocatalytic conversion of normal prion protein (PrP^{C}) to PrP^{Sc} (1, 2), known as the protein-only hypothesis. Some biophysical properties are known to differ between PrP^{C} and PrP^{Sc}. PrP^{C} is monomeric, detergent soluble, and protease sensitive, while PrP^{Sc} is polymeric, detergent insoluble, and partially protease resistant (3). These differences are most likely due to the different conformations of the two isoforms. PrP^{C} is largely α-helical, whereas PrP^{Sc} is substantially enriched in β-sheets (4, 5), frequently resulting in amyloid fibril formation.

The existence of diverse prion strains in mammalian species manifesting as phenotypic differences is well-known. The strain-specific characteristics are usually maintained upon serial passage in the same species and may be explained by conformational variations in PrP^{Sc}. Indeed, strain-dependent differences in β-sheet-rich structures of PrP^{Sc} have been demonstrated by infrared spectroscopy (6–9). In addition, the conformational stability of PrP^{Sc} differs among prion strains, as demonstrated by a guanidine hydrochloride (GdnHCl) denaturation assay followed by protease digestion (10, 11). However, the mechanistic relationship between

Received 26 February 2014 Accepted 26 July 2014
Published ahead of print 30 July 2014
Editor: B. W. Caughey
Address correspondence to Ryuichiro Atarashi, atarashi@nagasaki-u.ac.jp.

doi:10.1128/JVI.00585-14

PrP^{Sc} conformational differences and the molecular basis of prion strains remains poorly understood.

Various *in vitro* PrP^{Sc} formation methods have been developed to elucidate the pathogenesis of prion diseases. One of these methods, protein misfolding cyclic amplification (PMCA), enabled the exponential amplification of PrP^{Sc} *in vitro* by sonication-induced fragmentation of large PrP^{Sc} polymers into smaller units (12). An increase in the infectivity of PrP^{Sc} amplified by PMCA was obtained by using brain homogenate (BH) from healthy mice (normal brain homogenate [NBH]) as a source of PrP^{C} substrates (BH-PMCA) (13). Furthermore, PrP^{Sc} generated by BH-PMCA from five different mouse prion strains retained the strain-specific properties (14). In addition, prion infectivity could be propagated when purified brain-derived PrP^{C} or baculovirus-derived PrP^{C} was used as the substrate in the presence of certain cofactors, such as nucleic acids and BH from PrP-deficient mice (15–17). These results provide strong evidence to support the protein-only hypothesis, but the structural basis of prion pathogenesis, including the tertiary structure of PrP^{Sc}, has not been fully clarified.

On the other hand, the use of *Escherichia coli*-derived purified recombinant PrP (rPrP) offers an advantage over the use of conformational analyses, which generally require target protein of high purity and a large quantity of the target protein. Spontaneously polymerized amyloid fibrils of rPrP have been reported to induce the accumulation of PrP^{Sc} in the brains of PrP-overexpressing transgenic (Tg) mice (18–20) and some wild-type hamsters (21); however, the incubation periods spanned no less than several hundred days, and none of the wild-type hamsters developed any neurological signs at first passage, indicating that the level of infectivity generated in these studies is very low. More recently, wild-type mice developed clinical disease typical of TSE at about 130 days after injection of proteinase K (PK)-resistant rPrP fibrils generated by unseeded PMCA in the presence of 1-palmitoyl-2-oleoylphosphatidylglycerol (POPG), a synthetic lipid molecule, and total liver RNA (22). Although these results were reproduced by the same group (23), others have reported that rPrP fibrils generated by the same method were unable to induce either neuropathological changes or the accumulation of PrP^{Sc} (24). Thus, the role of POPG and RNA in the *de novo* generation of infectious rPrP fibrils remains controversial.

Meanwhile, two different seeded PMCA reaction studies using rPrP as a substrate (rPrP-PMCA) have demonstrated the propagation of moderate levels of prion infectivity. One study showed that hamster rPrP can be converted to rPrP fibrils capable of inducing TSE in the presence of SDS, a synthetic anionic detergent, but there were great variations in the attack rate and the incubation period, which ranged from 119 to 401 days (25). Another study revealed that phosphatidylethanolamine (PE), a phospholipid found in biological membranes, enhances the conversion of mouse rPrP into rPrP fibrils capable of inducing TSE after about 400 days of incubation with a 100% attack rate (26, 27). Of note, three different strains used as a seed were converted into a single strain with unique properties during the serial rPrP-PMCA experiments (27). These studies suggest that a certain amphipathic molecule, such as PE, is a cofactor required for the propagation of prion infectivity *in vitro* but not for the transmission of strain-specific properties.

The recently developed real-time (RT) quaking-induced conversion (QUIC) is a sensitive prion detection method (28, 29) in which intermittent shaking enhances the conversion of soluble rPrP into amyloid fibrils in the presence of PrP^{Sc}. The aim of the present research was to investigate whether properties of diverse prion strains can be transmitted to rPrP fibrils generated in the RT-QUIC system. We produced proteinase K-resistant rPrP fibrils seeded with minute quantities of mouse-adapted scrapie (Chandler or 22L strain) PrP^{Sc} and investigated the secondary structure, conformational stability, and infectivity.

MATERIALS AND METHODS

Mouse rPrP expression and purification. Recombinant PrP (rPrP) equivalent to residues 23 to 231 of the mouse PrP sequence was expressed, refolded into a soluble form, and purified essentially as previously described (30). The concentration of rPrP was determined by measuring the absorbance at 280 nm. The purity of the final protein preparations was ≥99%, as estimated by SDS-PAGE, immunoblotting, and liquid chromatography-mass spectrometry (data not shown). After purification, aliquots of the proteins were stored at −80°C in 10 mM phosphate buffer, pH 6.8, or distilled water.

Preparation of brain homogenates. Brain tissues were homogenized at 10% (wt/vol) in ice-cold phosphate-buffered saline (PBS) supplemented with a protease inhibitor mixture (Roche) using a multibead shocker (Yasui Kikai, Osaka, Japan). After centrifugation at 2,000 × *g* for 2 min, supernatants were collected and frozen at −80°C until use. Total protein concentrations were determined by the bicinchoninic acid protein assay (Pierce). The PrP^{Sc} concentrations in the brain homogenates were estimated by dot blot analysis using a reference standard of rPrP, as previously described (31).

RT-QUIC experiments. We prepared reaction mixtures in a 96-well, optical, black-bottom plate (catalog number 265301; Nunc) to a final total volume of 100 μl. To avoid contamination, we prepared noninfectious materials inside a biological safety cabinet in a prion-free laboratory and used aerosol-resistant tips. The final concentrations of the reaction buffer components were 300 mM NaCl, 50 mM HEPES, pH 7.5, and 10 μM thioflavin T (ThT). The concentration of rPrP was 50 or 100 μg/ml, and only freshly thawed rPrP was used. Brain homogenate was diluted with reaction buffer prior to the reactions. The 96-well plate was covered with sealing tape (catalog number 236366; Nunc) and incubated at 40°C in a plate reader (Infinite M200 fluorescence plate reader; Tecan) with intermittent shaking consisting of 30 s of circular shaking at the highest speed and no shaking for 30 s and then with a 2-min pause to measure the fluorescence. The kinetics of amyloid formation was monitored by reading of the fluorescence intensity on the bottom of the plate every 10 min using monochromators with 440-nm excitation and 485-nm emission wavelengths.

RT-QUIC product analysis. For detection of protease-resistant rPrP, 10 μl of the QUIC samples (1 μg of rPrP) was diluted with 40 μl of buffer (300 mM NaCl, 50 mM HEPES, pH 7.5) and digested with 10 μg/ml of PK at 37°C for 1 h. After adding 4-(2-aminoethyl)benzenesulfonyl fluoride hydrochloride (Pefabloc; Roche) at a final concentration of 4 mM and 20 μg of thyroglobulin, the proteins were precipitated with 4 volumes of methanol. The samples were heated in sample buffer (2% SDS, 5% β-mercaptoethanol, 5% sucrose, 0.005% bromophenol blue, 62.5 mM Tris-HCl, pH 6.8) at 95°C for 5 min and then loaded onto 10% bis-Tris NuPAGE gels (Invitrogen). Proteins were transferred onto polyvinylidene difluoride membranes (Millipore, Billerica, MA). The membranes were probed with polyclonal anti-PrP antibody R20 (the epitope located at mouse PrP amino acids 218 to 231) or ICSM35 (D-Gen, London, United Kingdom).

TEM. Negative staining was done on carbon supporting film grids, which were glow discharged before staining. The 10-μl samples were adsorbed to the grids for 3 min, and then the residual solution was absorbed by filter paper. The grids were stained with 20 μl of fleshly filtered stain (2% uranyl acetate). Once they were dry, the samples were viewed in a transmission electron microscope (TEM; JEM-1200EX; JEOL, Japan).

FTIR. Fourier transform infrared spectroscopy (FTIR) spectra were measured with a Bruker Tensor 27 FTIR instrument (Bruker Optics) equipped with a mercuric cadmium telluride (MCT) detector cooled with liquid nitrogen. Three hundred microliters of each of the QUIC samples (30 μg of rPrP) was pelleted by centrifugation for 1 h at 77,000 × *g* and resuspended in 20 μl buffer (300 mM NaCl, 50 mM HEPES, pH 7.5). The slurry was loaded into a BioATRcell II attenuated total reflectance-type reflectance unit. PrP^{Sc} was purified from the brains of mice infected with the mouse-adapted Chandler and 22L prions using a combination of detergent solubilization, centrifugation at ultrahigh speeds, and PK digestion (4, 32), and 15 μl of purified PrP^{Sc} was directly loaded. One hundred twenty-eight scans at a 4-cm^{-1} resolution were collected for each sample under constant purging with nitrogen, corrected for water vapor, and the background spectra of the buffer were subtracted.

Conformational stability assay. Ten microliters of the QUIC products (equivalent to 1 μg of rPrP) and brain homogenates (80 μg of total proteins) was mixed with 22 μl of various concentrations of guanidine hydrochloride (GdnHCl) at final concentrations of 0 to 5 M and 0 to 3.5 M, respectively, and the mixed samples were incubated at 37°C for 1 h. After adjustment of the final GdnHCl concentration of the QUIC products to 1 M and the brain homogenates to 0.6 M, the samples were digested with PK (10 μg/ml) at 37°C for 1 h and analyzed by Western blotting following methanol precipitation. The bands were visualized using an Attophos AP fluorescent substrate system (Promega) and quantified using a Molecular Imager FX imager (Bio-Rad). The sigmoidal patterns of the denaturation curves were plotted using a Boltzmann curve fit. The concentration of GdnHCl required to denature 50% of PK-resistant fragments ($[GdnHCl]_{1/2}$) was estimated from the denaturation curves.

Bioassay. Four-week-old male ddY mice were intracerebrally inoculated with 40 μl of QUIC products (equivalent to 4 μg rPrP). As controls for rPrP fibrils, we performed a mock QUIC procedure using seed-only solutions that contained the same concentration of PrP^{Sc} as that from the 1st round of QUIC with the rPrP fibril (1st-rPrP-fibril; 1 pg/μl) or the 5th round of QUIC with the rPrP fibril (5th-rPrP-fibril; 1×10^{-8} pg/μl) and then added the same amount of rPrP and inoculated the mixtures into mice. Brain homogenates were serially diluted from 10^{0} to 10^{-7} with PBS, and 20 μl of each dilution was intracerebrally inoculated. Mice were monitored weekly until the terminal stage of disease or sacrifice. Clinical onset was determined as the presence of 3 or more of the following signs: greasy and/or yellowish hair, hunchback, weight loss, yellow pubes, ataxic gait, and nonparallel hind limbs. The 50% lethal dose (LD_{50}) was determined according to the Behrens-Karber formula. Animals were cared for in accordance with the guidelines for animal experimentation of Nagasaki University.

Histopathology and lesion profiles. The brain tissue was fixed in 4% paraformaldehyde, and 5-μm paraffin sections were prepared on poly-L-lysine (PLL) coat slides using a microtome. After deparaffinization and rehydration, the tissue sections were stained with hematoxylin-eosin. The pattern of vacuolation was examined in 8 fields per slice from the hippocampus (HI), cerebral cortex, hypothalamus, pons, and cerebellum (CE). Spongiform degeneration was scored using the following scale: 0, no vacuoles; 1, a few vacuoles widely and unevenly distributed; 2, a few vacuoles evenly scattered; 3, moderate numbers of vacuoles evenly scattered; 4, many vacuoles with some confluences; and 5, dense vacuolation.

Statistical analysis. The fibril length or width determined by electron microscopy analysis was subjected to one-way analysis of variance (ANOVA) followed by the Tukey-Kramer test. Data from the conformational stability test were analyzed by one-way ANOVA followed by Student's *t* test. Analysis of the data for the survival times was evaluated by the log-rank test. The vacuolation scores were analyzed by Mann-Whitney's U test.

RESULTS

Conversion of the soluble form of mouse rPrP into amyloid fibrils by RT-QUIC. We first tested whether formation of mouse rPrP amyloid fibrils could be induced in the RT-QUIC by monitoring the levels of ThT fluorescence. We observed positive ThT fluorescence in the presence of diluted strain Chandler-seeded brain homogenate (BH) or strain 22L-seeded BH containing 100 pg of PrP^{Sc} (Fig. 1A), whereas negative-control reactions seeded with comparable dilutions of BH from healthy mice (normal brain homogenate [NBH]) or not seeded resulted in no increase in ThT fluorescence over 72 h (Fig. 1A). However, because an inverse correlation existed between the rate of fibril formation and the concentration of rPrP (28, 33), the spontaneous formation of rPrP fibrils (rPrP-fib^{spon}) was induced by decreasing the concentration of rPrP from 100 to 50 μg/ml (Fig. 1A).

We next examined the PK resistance of rPrP fibrils by immunoblotting using anti-PrP antibody R20 directed toward C-terminal residues 218 to 231. Although the ThT-negative reactions seeded with NBH or not seeded produced no PK-resistant bands (Fig. 1B, middle), the Chandler-seeded rPrP fibrils (rPrP-fib^{Ch}) and 22L-seeded rPrP fibrils (rPrP-fib^{22L}) produced several (21-, 18-, 12-, 11-, and 10-kDa) PK-resistant fragments (Fig. 1B, left). In contrast, the PK digestion of rPrP-fib^{spon} generated only 10- to 12-kDa fragments. It should be noted that anti-PrP monoclonal antibody ICSM35 (directed toward an epitope consisting of residues 93 to 102) specifically recognized the 21- and 18-kDa fragments derived from PrP^{Sc}-seeded rPrP fibrils in the first round (1st-rPrP-fib^{Sc}), indicating that they contained mouse PrP from about residues 93 to 231 (Fig. 1B, right).

To further characterize the structure of 1st-rPrP-fib^{Sc} and rPrP-fib^{spon}, the samples were examined using a TEM with negative staining. The electron micrographs of samples of 1st-rPrP-fib^{Ch} and 1st-rPrP-fib^{22L} revealed bundles of irregularly rod-shaped and branched fibrils, while most samples of rPrP-fib^{spon} displayed smooth and nonbranched rod-shaped fibrils (Fig. 1C). Moreover, the lengths of 1st-rPrP-fib^{Ch} and 1st-rPrP-fib^{22L} were significantly longer than those of rPrP-fib^{spon} (Fig. 1D). Thus, the results of TEM analysis suggest that 1st-rPrP-fib^{Sc} are structurally distinct from spontaneous rPrP-fib^{spon}.

We next examined the morphology of PrP^{Sc}-seeded rPrP fibrils in the 2nd- and 5th-round reactions (2nd- and 5th-rPrP-fib^{Sc}, respectively) by TEM. In contrast to samples of 1st-rPrP-fib^{Sc}, samples of 2nd- and 5th-rPrP-fib^{Sc} displayed spindly and nonbranched fibrils or amorphous aggregates (Fig. 2). These data support the view that 1st-rPrP-fib^{Sc} are structurally distinct from 2nd- and 5th-rPrP fib^{Sc}.

Structural characterization of rPrP fibrils by FTIR. We next examined the secondary structure of rPrP fibrils and purified PrP^{Sc} from the brains of mice infected with Chandler or 22L scrapie by FTIR. A silver-stained SDS-polyacrylamide gel analysis revealed that Chandler and 22L PrP^{Sc} preparations were highly purified (Fig. 3A). Furthermore, TEM analysis demonstrated that the PrP^{Sc} preparations consisted exclusively of amyloid-like fibrils (Fig. 3B). FTIR analysis showed that Chandler PrP^{Sc} was characterized by a major band at 1,630 cm^{-1} in the β-sheet region of second-derivative spectra, while 22L PrP^{Sc} was characterized by two absorbance bands at 1,631 and 1,616 cm^{-1} (Fig. 4A), indicating that there were conformational differences in the β-sheet structures between Chandler and 22L PrP^{Sc}, as previously reported (7). Consistent with previous reports (6–9), bands of about 1,656 to 1,658 cm^{-1} were observed in both Chandler and 22L PrP^{Sc}. Although these bands were formerly attributed to an α-helix, recent studies using direct mass spectrometric analysis of hy-

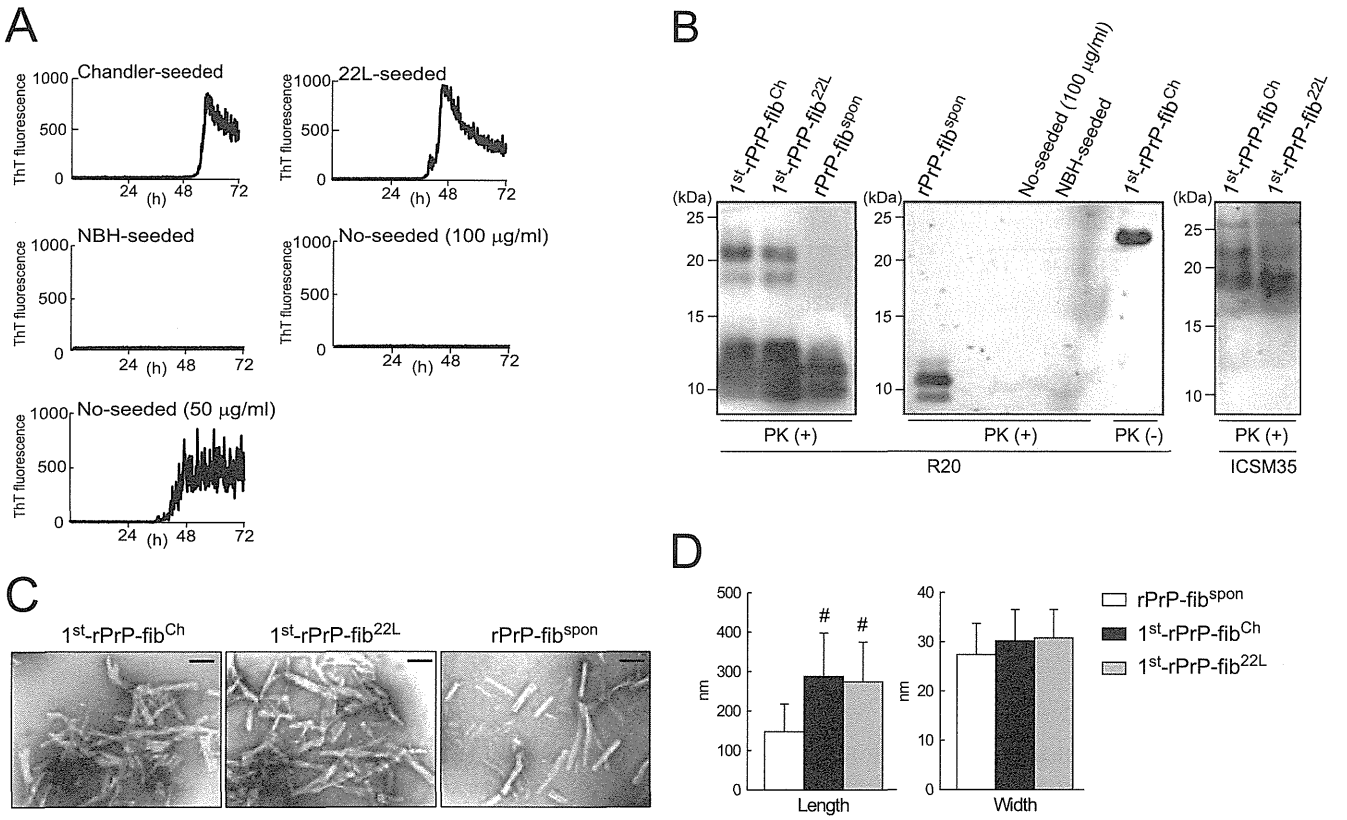

FIG 1 Formation of rPrP fibrils in RT-QUIC reactions. (A) The formation of rPrP fibrils in the presence of diluted Chandler or 22L BH containing 100 pg of PrP^{Sc} or a comparable amount of NBH or in the absence of seed (No-seeded) was monitored by measurement of ThT fluorescence. The graphs depict representative results of the RT-QUIC reactions. No-seed reactions were performed at two different concentrations (100 or 50 μg/ml) of rPrP. (B) The QUIC reaction mixtures were digested with PK and immunoblotted using polyclonal anti-PrP antibody R20 (specific for the epitope located at mouse PrP amino acids 218 to 231) or ICSM35 (specific for the epitope located at mouse PrP amino acids 93 to 102). For comparison, 1st-rPrP-fib^{Ch} (50 ng of total rPrP) without PK digestion [PK (−)] is shown. Molecular mass markers are indicated in kilodaltons (kDa) on the left side of each panel. (C) Samples (1st-rPrP-fib^{Ch}, 1st-rPrP-fib^{22L}, and rPrP-fib^{spon}) were examined by TEM. Bars, 100 nm. (D) The bar graph shows the length and width of rPrP-fib^{spon}, 1st-rPrP-fib^{Ch}, and 1st-rPrP-fib^{22L}. The results are the mean ± SD for 30 rPrP fibrils each. Statistical significance was determined using one-way ANOVA, followed by the Tukey-Kramer test. *, $P < 0.01$.

drogen-deuterium exchange and FTIR analysis have suggested that purified PrP^{Sc} has little α-helix content and the bands probably result from turns (9, 34). Native rPrP had a maximum absorbance at 1,653 cm^{-1}, which was congruent with that of prominent α-helical structures. In contrast, all rPrP fibrils displayed prominent bands at lower wave numbers (1,630 to 1,610 cm^{-1}), indicating a predominantly β-sheet content (Fig. 4A). The β-sheet spectra revealed conformational differences among rPrP-fib^{spon}, 1st-rPrP-fib^{Ch}, and 1st-rPrP-fib^{22L}. rPrP-fib^{spon} had a prominent band at 1,623 cm^{-1} and a modest band at 1,610 cm^{-1}. While the 1st-rPrP-fib^{Ch} were characterized by a single major band at 1,624 cm^{-1}, the 1st-rPrP-fib^{22L} had two major maxima at 1,629 and 1,617 cm^{-1} (Fig. 4A). Although 1st-rPrP-fib^{Sc} lacked the bands at about 1,656 to 1,658 cm^{-1}, the strain-specific shapes (one peak in Chandler versus two peaks in 22L) in the β-sheet spectrum of the purified PrP^{Sc} resembled those of 1st-rPrP-fib^{Sc}.

To test whether the strain-specific infrared spectra observed in 1st-rPrP-fib^{Ch} and 1st-rPrP-fib^{22L} are transmitted to sequential QUIC reactions, we performed 5 serial rounds of QUIC (Fig. 2A). There was little difference in the β-sheet spectra between 5th-rPrP-fib^{Ch} and 5th-rPrP-fib^{22L} (Fig. 3), suggesting that strain-specific conformations were lost in the 5th-rPrP-fib^{Sc}. Furthermore, additional experiments revealed that the infrared spectra of rPrP fibrils produced in the presence of a small amount of PrP^{Sc} (1 pg) or under acidic conditions (pH 4) displayed few differences between strains (Fig. 4B).

Conformational stability analysis of rPrP fibrils and PrP^{Sc}. To examine the biochemical differences of rPrP fibrils and PrP^{Sc} in BH between strains, we performed a conformational stability assay, which combines GdnHCl denaturation with PK digestion. The $[GdnHCl]_{1/2}$ values for Chandler and 22L PrP^{Sc} were 3.3 ± 0.4 and 1.7 ± 0.3 M, respectively (Fig. 5A and Table 1), indicating that the conformational stability of Chandler-PrP^{Sc} was significantly higher than that of 22L-PrP^{Sc}. Consistent with previous work (11), Chandler PrP^{Sc} bands treated with more than 1.5 M GdnHCl were approximately 5 kDa smaller than those treated with lower concentrations (Fig. 5A, top). The $[GdnHCl]_{1/2}$ values of 1st-rPrP-fib^{Ch} and 1st-rPrP-fib^{22L} were 3.3 ± 0.1 and 2.3 ± 0.6 M, respectively (Fig. 5B and Table 1), showing that the stability of 1st-rPrP-fib^{Ch} was significantly higher than that of 1st-rPrP-fib^{22L}, as with Chandler and 22L PrP^{Sc}. Thus, the relationship between Chandler and 22L in terms of conformational stability was common to both the original PrP^{Sc} and 1st-rPrP-fib^{Sc}. In contrast, the $[GdnHCl]_{1/2}$ of rPrP-fib^{spon} was more than 5 M,

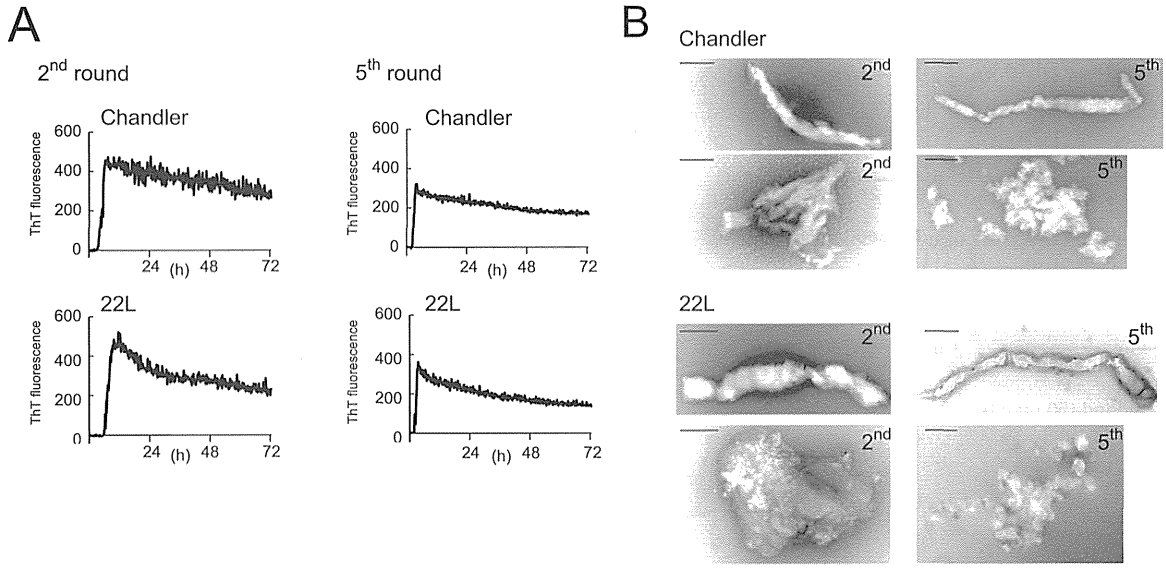

FIG 2 Formation of PrP^{Sc}-seeded rPrP fibrils in the 2nd round (2nd-rPrP-fib^{Sc}) and 5th round (5th-rPrP-fib^{Sc}) of RT-QUIC. (A) Between each round, the reaction mixtures from the previous reaction were diluted 100-fold into fresh rPrP. The reaction buffer contained 300 mM NaCl, 50 mM HEPES (pH 7.5), and 10 μM ThT. The rPrP concentration was 100 μg/ml. (B) TEM analysis of PrP^{Sc}-seeded rPrP fibrils generated in the second and fifth rounds of RT-QUIC. Bars, 100 nm.

which was markedly higher than that of 1st-rPrP-fib^{Sc} (Fig. 5B and Table 1). Additionally, we tested the conformational stability of 2nd- and 5th-rPrP-fib^{Sc} but found no significant differences between strains (Fig. 5C and D and Table 1).

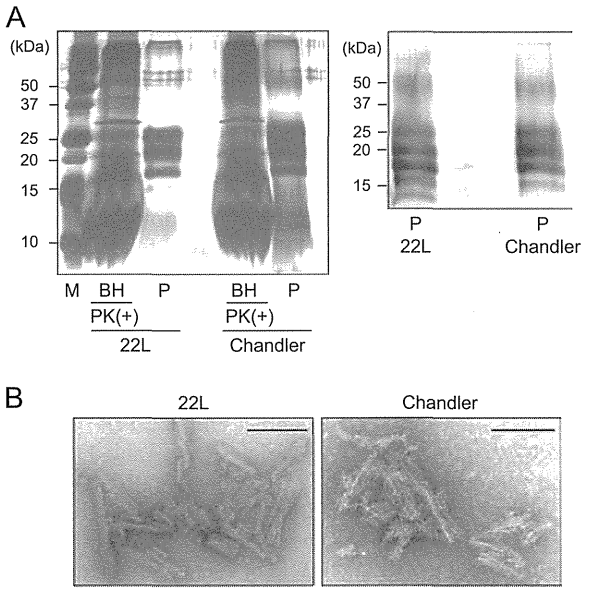

FIG 3 Silver staining and Western blot analysis of purified PrP^{Sc}. (A) The purified PrP^{Sc} samples (P) were examined by silver-stained SDS-polyacrylamide gel analysis (left). For comparison, the electrophoretic pattern of prion-infected BHs containing 100 μg total protein digested with PK (20 μg/ml, 37°C for 1 h) is shown (left). The purified PrP^{Sc} samples were immunoblotted with polyclonal anti-PrP antibody M20 (right). Molecular mass markers (lane M) are indicated in kilodaltons (kDa) on the left side of each panel. (B) Electron microscopy analysis of purified 22L PrP^{Sc} (left) and Chandler PrP^{Sc} (right). Bars, 100 nm.

Bioassay for rPrP fibrils generated in QUIC reactions. To determine whether the infectivity was transmitted to the rPrP fibrils, we performed a bioassay using wild-type mice. To prepare the control materials, seed-only solutions containing the same concentration of PrP^{Sc} as that in 1st- or 5th-rPrP-fib^{Sc} were subjected to a mock RT-QUIC procedure and then mixed with the same amount of soluble rPrP (Table 2). The survival periods of mice inoculated with 40-μl aliquots containing rPrP fibrils were 185.5 ± 4.0 days postinoculation (dpi) for 1st-rPrP-fib^{Ch} and 213.0 ± 8.9 dpi for 1st-rPrP-fib^{22L} (Table 2). In contrast, the attack rate of these control mice was only 50% (2/4) for Chandler and 20% (1/5) for 22L. Moreover, the survival period of the affected mice was much longer than that of the mice inoculated with 1st-rPrP-fib^{Sc} (Table 2). For comparison with the 50% lethal dose (LD_{50}) of the original PrP^{Sc}, the LD_{50} of 1st-rPrP-fib^{Sc} was determined from the linear regression relationship between infectious titers and survival periods. The infectious titers (per 40 μl) of 1st-rPrP-fib^{Ch} and 1st-rPrP-fib^{22L} were estimated to be 407.2 ± 226.6 and 1,067.0 ± 678.7 LD_{50}s, respectively, whereas the titers of the Chandler and 22L prions were 20.2 and 28.9 LD_{50} units/40 pg of PrP^{Sc}, respectively. Because the QUIC reaction in the first round resulted in a 20- to 37-fold increase in the infectious titer, the seed contribution to infectivity is estimated to be about 3 to 5%. In contrast, none of the mice inoculated with 5th-rPrP-fib^{Sc} developed symptoms related to TSE (Table 2), suggesting that the 5th-rPrP-fib^{Sc} has no substantial infectivity.

We analyzed by Western blotting the levels of PrP^{Sc} in the brain tissues of mice in the terminal stage that had been inoculated with 1st-rPrP-fib^{Sc} or control materials (mock 1st QUIC) and found no apparent differences in the accumulation of PrP^{Sc} between them and mice inoculated with mock 1st QUIC (Fig. 6A). In addition, a conformational stability assay with GdnHCl revealed that the strain-specific digestion pattern was preserved in mice inoculated with 1st-rPrP-fib^{Sc} (Fig. 6B).

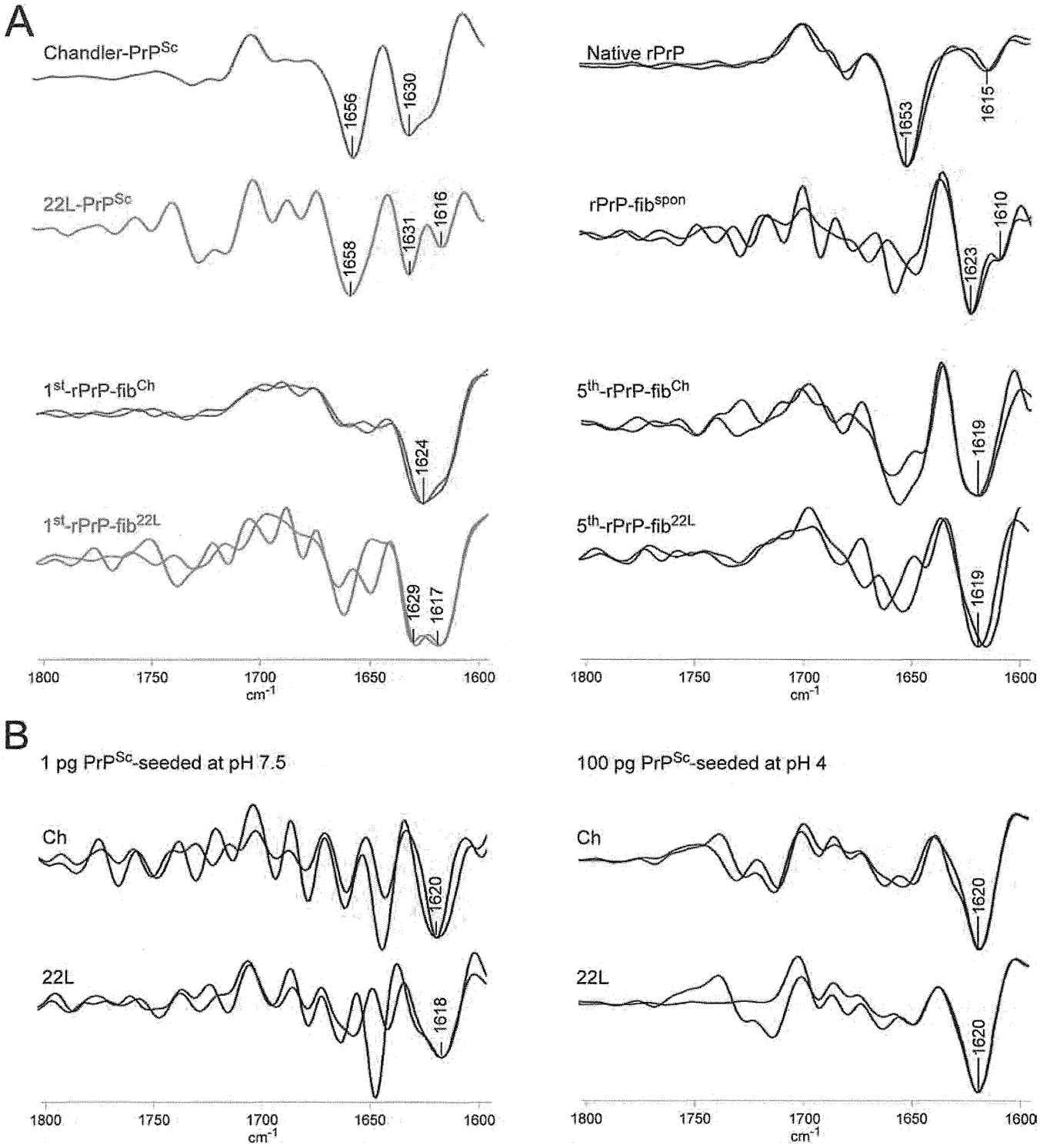

FIG 4 FTIR spectroscopic characterization of rPrP fibrils and purified PrP^{Sc}. (A) Second-derivative FTIR spectra are shown for purified PrP^{Sc}, 1st-rPrP-fib^{Sc}, 5th-rPrP-fib^{Sc}, spontaneously formed rPrP fibrils (rPrP-fib^{spon}), and native rPrP. Overlaid spectra are from independent preparations. (B) FTIR spectra of rPrP fibrils generated at pH 7.5 in the presence of a small amount (1 pg) of PrP^{Sc} and rPrP fibrils generated at pH 4 in the presence of 100 pg of PrP^{Sc}.

Next, the degree of vacuolation in brain sections, including the hippocampus (HI), cerebral cortex, thalamus, pons, and cerebellum (CE), from affected mice inoculated with 1st-rPrP-fib^{Sc} or mock 1st QUIC and those inoculated with the second passage of 1st-rPrP-fib^{Sc} was examined histologically (Fig. 6C and D). Of note, we found that the spongiform change in mice inoculated with 1st-rPrP-fib^{Sc} was less severe in the HI and CE than that in the HI and CE of mice inoculated with mock 1st QUIC strains (Fig. 6C

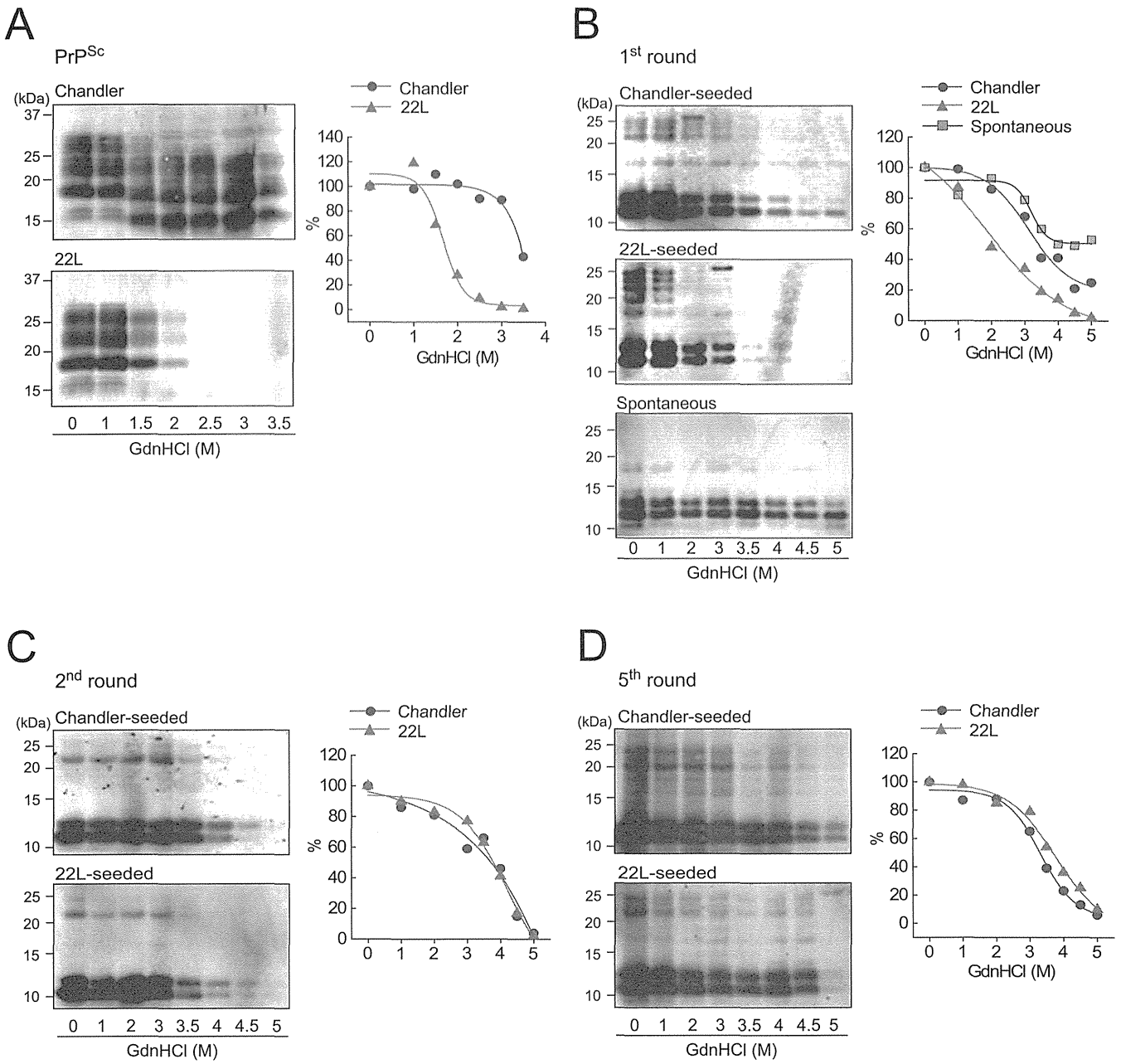

FIG 5 Conformational stability assay for PrP^{Sc} in BH and rPrP fibrils. (A) Chandler-infected (top left) or 22L-infected (bottom left) BHs were treated with 0 to 3.5 M GdnHCl and subjected to PK digestion. PrP^{Sc} was detected by R20 anti-PrP polyclonal antibody. The denaturation curves were plotted using Boltzmann curve fitting (right). (B to D) PK-digested 1st-rPrP-fib^{Sc} (generated as described in the legend to Fig. 1) and rPrP-fib^{spon} (B), 2nd-rPrP-fib^{Sc} (C), or 5th-rPrP-fib^{Sc} (D) were analyzed by Western blotting following GdnHCl treatment (0 to 5 M). The PK-resistant fragments of the rPrP fibrils were detected by antibody R20.

TABLE 1 Conformational stabilities of purified PrP^{Sc} and rPrP fibrils[a]

Strain	$[GdnHCl]_{1/2}$ (mol/liter)			
	Purified PrP^{Sc}	rPrP fibrils		
		1st	2nd	5th
Chandler	3.3 ± 0.4**	3.3 ± 0.1*	3.7 ± 0.1	3.3 ± 0.3
22L	1.7 ± 0.3	2.3 ± 0.6	3.8 ± 0.2	3.5 ± 1.0
Spontaneous		>5		

[a] The $[GdnHCl]_{1/2}$ values (mol/liter) are means ± standard deviations from three independent experiments. Statistical significance was determined using one-way ANOVA, followed by Student's *t* test. **, $P < 0.01$ (compared with 22L); *, $P < 0.05$ (compared with 22L).

and D). Furthermore, these different lesion profiles observed in mice inoculated with 1st-rPrP-fib^{Sc} were preserved upon second passage (Fig. 6D), suggesting that the characters of 1st-rPrP-fib^{Sc} are partially distinct from those of the original strains. These findings support the notion that 1st-rPrP-fib^{Sc} provoke the emergence of a mutant strain beyond seed-derived infectivity.

DISCUSSION

Recent studies show that RT-QUIC assays are useful for the sensitive detection of PrP^{Sc} in most species and strains, including

TABLE 2 Bioassay for rPrP fibrils generated in QUIC reactions in wild-type mice[a]

Inoculum	Concn of seed PrP^{Sc} (pg/μl)	Survival period (dpi)[b]	Mortality (no. of dead mice/ total no. tested)
1st-rPrP-fib^{Ch}	1	185.5 ± 4.0*[d]	4/4
Mock 1st QUIC (Ch)[c]	1	201, 220[e]	2/4
1st-rPrP-fib^{22L}	1	213.0 ± 8.9**[d]	6/6
Mock 1st QUIC (22L)[c]	1	333[e]	1/5
5th-rPrP-fib^{Ch}	1×10^{-8}	>660[f]	0/4
Mock 5th QUIC (Ch)[c]	1×10^{-8}	>660[f]	0/4
5th-rPrP-fib^{22L}	1×10^{-8}	>660[f]	0/6
Mock 5th QUIC (22L)[c]	1×10^{-8}	>660[f]	0/6
rPrP-fib^{spon}	0	>660[f]	0/6
Second passage of 1st-rPrP-fib^{Ch}		152.0 ± 8.5[d]	5/5
Second passage of mock 1st QUIC (Ch)[g]		148.4 ± 5.9[d]	5/5
Second passage of 1st-rPrP-fib^{22L}		153.5 ± 0.6[d]	5/5
Second passage of mock 1st QUIC (22L)[h]		149.6 ± 10.4[d]	4/4

[a] Mice were intracerebrally inoculated with 40 μl of each inoculum. For the second passage, 10% BH was used.
[b] Statistical significance was determined using the log rank test. **, $P < 0.01$ (compared with the controls); *, $P < 0.05$ (compared with the controls). dpi, days postinoculation.
[c] After subjecting seed-only mixtures containing the same concentration of PrP^{Sc} as 1st- or 5th-rPrP-fib^{Sc} to a mock QUIC procedure, the same amount of rPrP was added. The solutions were inoculated into mice as controls for rPrP fibrils.
[d] Data represent means ± standard deviations.
[e] Data represent the survival periods of the TSE-positive mice. All nonsymptomatic mice were negative for PrP^{Sc} at 660 dpi.
[f] Data represent the day postinoculation when the experiment was ended.
[g] A sample from a mouse obtained at 201 dpi was used.
[h] A sample from a mouse obtained at 333 dpi was used.

Creutzfeldt-Jakob disease (CJD) in humans (28, 35–37), scrapie in rodents (29, 38), and chronic wasting disease (CWD) in cervids (39). In the RT-QUIC reaction, soluble rPrP is converted to amyloid fibrils in a seed-dependent fashion in the presence of PrP^{Sc}. Previous studies using FTIR and hydrogen-deuterium exchange have shown that there are structural differences between PrP^{Sc}-seeded fibrils and spontaneous rPrP fibrils generated in rPrP amplified by PMCA (7, 40). We also found that the structural morphology (Fig. 1C), secondary structure (Fig. 3), and conformational stability (Fig. 4B and Table 1) distinguish 1st-rPrP-fib^{Sc} from rPrP-fib^{spon}. However, it has been unknown whether rPrP retains the conformational properties of the original PrP^{Sc} in the RT-QUIC. Consistent with previous reports (7, 11), we observed strain differences in the β-sheet structure and conformational stability of PrP^{Sc} between the Chandler and 22L strains. Likewise, the differences in the shape of the β-sheet spectrum between strains were common to both PrP^{Sc} and 1st-rPrP-fib^{Sc}. Furthermore, the conformational stability of 1st-rPrP-fib^{22L} was significantly lower than that of 1st-rPrP-fib^{Ch}, as was the case with Chandler and 22L PrP^{Sc}. Since the original PrP^{Sc} remaining in 1st-rPrP-fib^{Sc} was equivalent to only about 0.01 to 0.02% of the PK-resistant 1st-rPrP-fib^{Sc} (1 to 2 μg/10 μg of total PrP) in our estimation, the contribution to the FTIR spectra and the conformational stability of 1st-rPrP-fib^{Sc} are considered to be negligible. Taken together, these studies demonstrate that at least some strain-specific conformational features, especially in the β-sheet region, are conserved between PrP^{Sc} and 1st-rPrP-fib^{Sc}. However, these unique structural features disappeared in subsequent rounds.

One of the reasons for the loss of strain specificity may be due to differences between *E. coli*-derived rPrP and brain-derived PrP^{C}. Studies using circular dichroism and ^{1}H nuclear magnetic resonance spectroscopy showed that the tertiary structure and the thermal stability of bovine rPrP from positions 23 to 230 are essentially identical to those of healthy calf brain-derived PrP^{C} (41). However, it should be noted that *E. coli*-derived rPrP lacks posttranslational modifications of PrP^{C}, such as glycosylation and a glycosylphosphatidylinositol (GPI) anchor. PrP has two N-linked glycosylation sites at amino acids 180 and 196, resulting in di-, mono-, and unglycosylated forms. Mature PrP^{C} is rich in the diglycosylated form, whereas the glycoform ratio of PrP^{Sc} is known to vary among strains (42–44). Studies using PrP glycan-lacking Tg mice revealed that the strain-specific characteristics of strain 79A were affected by the glycosylation status of PrP^{C}, but those of strains ME7 and 301C were not (45). Meanwhile, enzymatic deglycosylation of PrP^{C} failed to affect strain-specific pathological changes in serial PMCA experiments seeded with two murine strains, RML and 301C (46). However, the same two strains were converted into a new single strain during serial rPrP-PMCA in the presence of synthetic PE (27). Similarly, the emergence of mutant strains whose lesion profiles differed from the lesion profile of the seed strain was also observed in a bioassay using hamster rPrP fibrils generated in seeded rPrP-PMCA (25) or 1st-rPrP-fib^{Sc} (Fig. 6C and D). These results raise the possibility that the lack of a GPI anchor in rPrP leads to alterations in strain-specific characteristics. Furthermore, the cell tropisms determined by the cell panel assay were altered in strains RML, 139A, 79A, and ME7 but not in strain 22L when the strains were propagated in Tg mice expressing PrP devoid of a GPI anchor (47). These studies demonstrate that glycosylation and a GPI anchor are not necessarily required for the propagation of prion infectivity but can influence the strain properties. Although the molecular basis of the emergence of mutant strains remains elusive, we can speculate that the posttranslational changes to PrP might affect the conformation of PrP^{Sc} or the interaction with some cofactor(s) in a strain-specific manner.

Another possible explanation is that nonspecific rPrP fibrils are generated during the serial RT-QUIC and replicate more rapidly than the fibrils with strain-specific conformations. The term "nonspecific rPrP fibrils" arises from our findings that there was little difference in the infrared spectra and conformational stability of 5th-rPrP-fib^{Sc} between strains. It has been reported that the propagation of prion strains in cells cultured under different environmental conditions often leads to the formation of quasispecies that are assumed to be composed of a variety of conformational variants (48, 49). Once generated, the competition among the variants is thought to occur during propagation. Indeed, two conformational variants of rPrP fibrils have been shown to be mutually exclusive and compete for monomeric rPrP as a substrate in fibril formation (30). Furthermore, competitive amplification of two prion strains was demonstrated by BH-PMCA (50). Similarly, nonspecific rPrP fibrils would be expected to become the majority if they had a selective growth advantage in the RT-QUIC. We found that the β-sheet spectra of rPrP fibrils generated in the presence of a small amount (1 pg) of PrP^{Sc} or rPrP fibrils

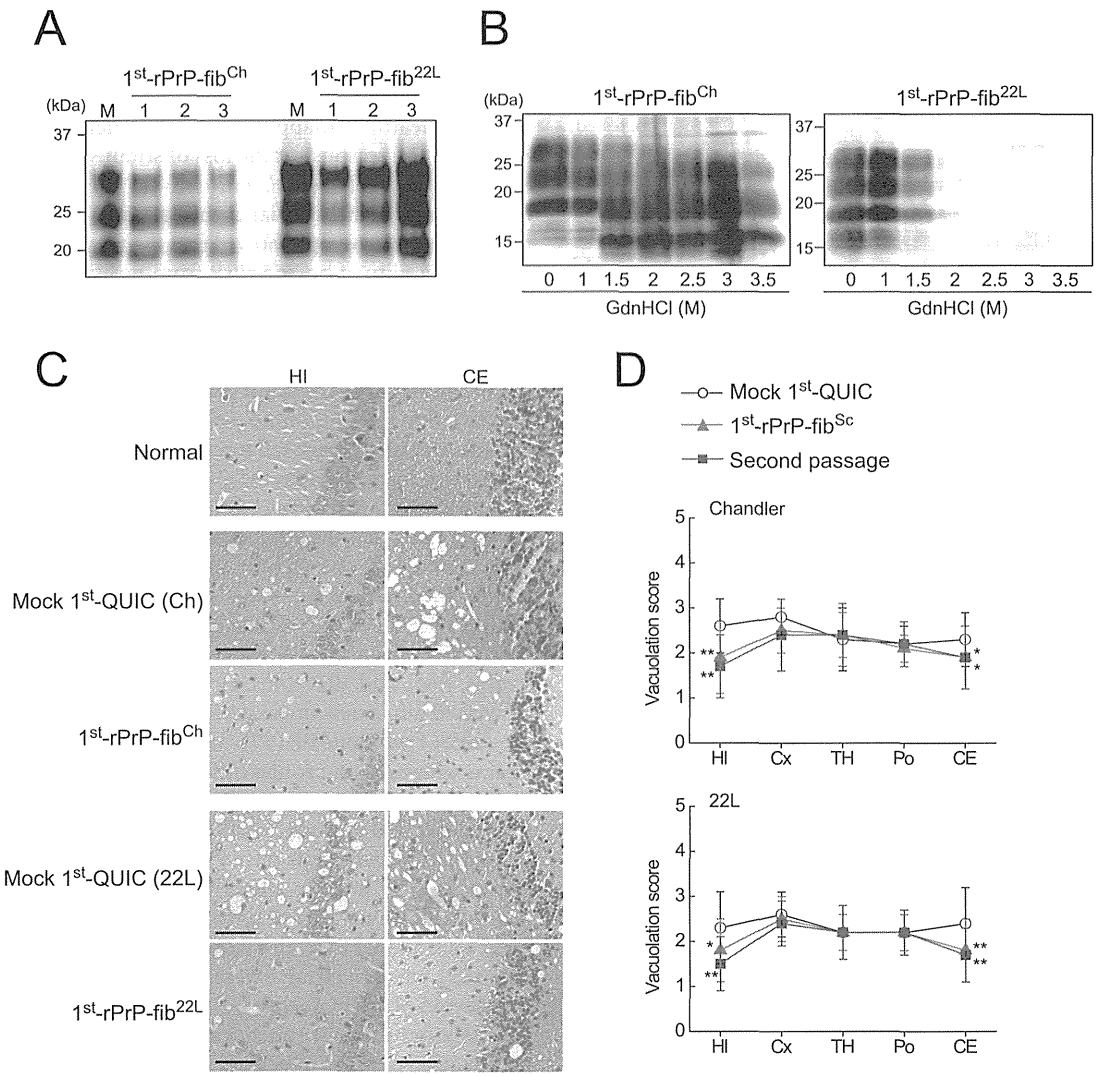

FIG 6 Bioassay of rPrP fibrils in mice. (A) PrP^{Sc} in the brains of prion-affected mice inoculated with 1st-rPrP-fib^{Ch} or 1st-rPrP-fib^{22L} was analyzed by Western blotting using anti-PrP antibody M20. Lanes M, mock 1st QUIC for strains Chandler and 22L. (B) The strain-specific properties of PrP^{Sc} in the brains of mice inoculated with 1st-rPrP-fib^{Sc} were examined by a conformational stability assay with GdnHCl (0 to 3.5 M). (C) Sections of the hippocampus (HI) and cerebellum (CE), stained with hematoxylin-eosin, from healthy mice, mice inoculated with 1st-rPrP-fib^{Sc}, and mock 1st QUIC-inoculated mice at terminal stages are shown. Bars, 50 μm. (D) Lesion profiles of spongiform changes in the hippocampus, cerebral cortex (Cx), thalamus (TH), pons (Po), and cerebellum were compared. Data are expressed as means ± SDs ($n = 3$). Statistical significance was determined using Mann-Whitney's U test. **, $P < 0.01$; *, $P < 0.05$.

generated at pH 4 in the first round were similar to those seen for 5th-rPrP-fib^{Sc} (Fig. 4B). These observations also support this hypothesis and suggest that the amplification of nonspecific rPrP fibrils is accelerated by certain conditions, such as an acidic environment. Further studies are needed to investigate whether unknown cofactors or environmental conditions are required to maintain the strain-specific conformations in subsequent rounds. On the other hand, this hypothesis also explains why prion infectivity was lost in the fifth round of RT-QUIC, as nonspecific rPrP fibrils generated during the serial RT-QUIC would be noninfectious. Although there remains the question as to what exactly the conformational differences between the noninfectious and infectious forms of rPrP fibrils are, the lack of cofactor molecules, such as SDS and synthetic PE, in the RT-QUIC might enhance the amplification of nonspecific rPrP fibrils lacking prion infectivity. Moreover, the fact that prion infectivity is sometimes too low to be detected and, more frequently, the fact that prion infectivity declines in the serial rPrP-PMCA (24, 25) or BH-PMCA (51–53) are consistent with the hypothesis.

ACKNOWLEDGMENTS

We thank Takashi Suematsu for help with the electron microscopy study and Matsuo Atsuko and Ayumi Yamakawa for technical assistance.

This work was supported by a grant-in-aid for young scientists (B; grant no. 21790846) from the Ministry of Education, Culture, Sports, Science and Technology of Japan, a grant for BSE research, and a grant-in-aid from the Research Committee of Prion Disease and Slow Virus Infection from the Ministry of Health, Labor and Welfare of Japan.

REFERENCES

1. **Prusiner SB.** 1991. Molecular biology of prion diseases. Science 252: 1515–1522. http://dx.doi.org/10.1126/science.1675487.

2. Weissmann C, Enari M, Klohn PC, Rossi D, Flechsig E. 2002. Molecular biology of prions. Acta Neurobiol. Exp. (Wars.) 62:153–166.
3. Meyer RK, McKinley MP, Bowman KA, Braunfeld MB, Barry RA, Prusiner SB. 1986. Separation and properties of cellular and scrapie prion proteins. Proc. Natl. Acad. Sci. U. S. A. 83:2310–2314. http://dx.doi.org/10.1073/pnas.83.8.2310.
4. Caughey BW, Dong A, Bhat KS, Ernst D, Hayes SF, Caughey WS. 1991. Secondary structure analysis of the scrapie-associated protein PrP 27-30 in water by infrared spectroscopy. Biochemistry 30:7672–7680. http://dx.doi.org/10.1021/bi00245a003.
5. Pan KM, Baldwin M, Nguyen J, Gasset M, Serban A, Groth D, Mehlhorn I, Huang Z, Fletterick RJ, Cohen FE, Prusiner SB. 1993. Conversion of alpha-helices into beta-sheets features in the formation of the scrapie prion proteins. Proc. Natl. Acad. Sci. U. S. A. 90:10962–10966. http://dx.doi.org/10.1073/pnas.90.23.10962.
6. Caughey B, Raymond GJ, Bessen RA. 1998. Strain-dependent differences in beta-sheet conformations of abnormal prion protein. J. Biol. Chem. 273:32230–32235. http://dx.doi.org/10.1074/jbc.273.48.32230.
7. Atarashi R, Sim VL, Nishida N, Caughey B, Katamine S. 2006. Prion strain-dependent differences in conversion of mutant prion proteins in cell culture. J. Virol. 80:7854–7862. http://dx.doi.org/10.1128/JVI.00424-06.
8. Thomzig A, Spassov S, Friedrich M, Naumann D, Beekes M. 2004. Discriminating scrapie and bovine spongiform encephalopathy isolates by infrared spectroscopy of pathological prion protein. J. Biol. Chem. 279:33847–33854. http://dx.doi.org/10.1074/jbc.M403730200.
9. Baron GS, Hughson AG, Raymond GJ, Offerdahl DK, Barton KA, Raymond LD, Dorward DW, Caughey B. 2011. Effect of glycans and the glycophosphatidylinositol anchor on strain dependent conformations of scrapie prion protein: improved purifications and infrared spectra. Biochemistry 50:4479–4490. http://dx.doi.org/10.1021/bi2003907.
10. Peretz D, Scott MR, Groth D, Williamson RA, Burton DR, Cohen FE, Prusiner SB. 2001. Strain-specified relative conformational stability of the scrapie prion protein. Protein Sci. 10:854–863. http://dx.doi.org/10.1110/ps.39201.
11. Shindoh R, Kim CL, Song CH, Hasebe R, Horiuchi M. 2009. The region approximately between amino acids 81 and 137 of proteinase K-resistant PrPSc is critical for the infectivity of the Chandler prion strain. J. Virol. 83:3852–3860. http://dx.doi.org/10.1128/JVI.01740-08.
12. Saborio GP, Permanne B, Soto C. 2001. Sensitive detection of pathological prion protein by cyclic amplification of protein misfolding. Nature 411:810–813. http://dx.doi.org/10.1038/35081095.
13. Castilla J, Saa P, Hetz C, Soto C. 2005. In vitro generation of infectious scrapie prions. Cell 121:195–206. http://dx.doi.org/10.1016/j.cell.2005.02.011.
14. Castilla J, Morales R, Saa P, Barria M, Gambetti P, Soto C. 2008. Cell-free propagation of prion strains. EMBO J. 27:2557–2566. http://dx.doi.org/10.1038/emboj.2008.181.
15. Deleault NR, Harris BT, Rees JR, Supattapone S. 2007. Formation of native prions from minimal components in vitro. Proc. Natl. Acad. Sci. U. S. A. 104:9741–9746. http://dx.doi.org/10.1073/pnas.0702662104.
16. Imamura M, Kato N, Yoshioka M, Okada H, Iwamaru Y, Shimizu Y, Mohri S, Yokoyama T, Murayama Y. 2011. Glycosylphosphatidylinositol anchor-dependent stimulation pathway required for generation of baculovirus-derived recombinant scrapie prion protein. J. Virol. 85:2582–2588. http://dx.doi.org/10.1128/JVI.02098-10.
17. Imamura M, Kato N, Okada H, Yoshioka M, Iwamaru Y, Shimizu Y, Mohri S, Yokoyama T, Murayama Y. 2013. Insect cell-derived cofactors become fully functional after proteinase K and heat treatment for high-fidelity amplification of glycosylphosphatidylinositol-anchored recombinant scrapie and BSE prion proteins. PLoS One 8:e82538. http://dx.doi.org/10.1371/journal.pone.0082538.
18. Legname G, Baskakov IV, Nguyen HO, Riesner D, Cohen FE, DeArmond SJ, Prusiner SB. 2004. Synthetic mammalian prions. Science 305:673–676. http://dx.doi.org/10.1126/science.1100195.
19. Colby DW, Giles K, Legname G, Wille H, Baskakov IV, DeArmond SJ, Prusiner SB. 2009. Design and construction of diverse mammalian prion strains. Proc. Natl. Acad. Sci. U. S. A. 106:20417–20422. http://dx.doi.org/10.1073/pnas.0910350106.
20. Raymond GJ, Race B, Hollister JR, Offerdahl DK, Moore RA, Kodali R, Raymond LD, Hughson AG, Rosenke R, Long D, Dorward DW, Baron GS. 2012. Isolation of novel synthetic prion strains by amplification in transgenic mice coexpressing wild-type and anchorless prion proteins. J. Virol. 86:11763–11778. http://dx.doi.org/10.1128/JVI.01353-12.
21. Makarava N, Kovacs GG, Bocharova O, Savtchenko R, Alexeeva I, Budka H, Rohwer RG, Baskakov IV. 2010. Recombinant prion protein induces a new transmissible prion disease in wild-type animals. Acta Neuropathol. 119:177–187. http://dx.doi.org/10.1007/s00401-009-0633-x.
22. Wang F, Wang X, Yuan CG, Ma J. 2010. Generating a prion with bacterially expressed recombinant prion protein. Science 327:1132–1135. http://dx.doi.org/10.1126/science.1183748.
23. Zhang Z, Zhang Y, Wang F, Wang X, Xu Y, Yang H, Yu G, Yuan C, Ma J. 2013. De novo generation of infectious prions with bacterially expressed recombinant prion protein. FASEB J. 27:4768–4775. http://dx.doi.org/10.1096/fj.13-233965.
24. Timmes AG, Moore RA, Fischer ER, Priola SA. 2013. Recombinant prion protein refolded with lipid and RNA has the biochemical hallmarks of a prion but lacks in vivo infectivity. PLoS One 8:e71081. http://dx.doi.org/10.1371/journal.pone.0071081.
25. Kim JI, Cali I, Surewicz K, Kong Q, Raymond GJ, Atarashi R, Race B, Qing L, Gambetti P, Caughey B, Surewicz WK. 2010. Mammalian prions generated from bacterially expressed prion protein in the absence of any mammalian cofactors. J. Biol. Chem. 285:14083–14087. http://dx.doi.org/10.1074/jbc.C110.113464.
26. Deleault NR, Piro JR, Walsh DJ, Wang F, Ma J, Geoghegan JC, Supattapone S. 2012. Isolation of phosphatidylethanolamine as a solitary cofactor for prion formation in the absence of nucleic acids. Proc. Natl. Acad. Sci. U. S. A. 109:8546–8551. http://dx.doi.org/10.1073/pnas.1204498109.
27. Deleault NR, Walsh DJ, Piro JR, Wang F, Wang X, Ma J, Rees JR, Supattapone S. 2012. Cofactor molecules maintain infectious conformation and restrict strain properties in purified prions. Proc. Natl. Acad. Sci. U. S. A. 109:E1938–E1946. http://dx.doi.org/10.1073/pnas.1206999109.
28. Atarashi R, Satoh K, Sano K, Fuse T, Yamaguchi N, Ishibashi D, Matsubara T, Nakagaki T, Yamanaka H, Shirabe S, Yamada M, Mizusawa H, Kitamoto T, Klug G, McGlade A, Collins SJ, Nishida N. 2011. Ultrasensitive human prion detection in cerebrospinal fluid by real-time quaking-induced conversion. Nat. Med. 17:175–178. http://dx.doi.org/10.1038/nm.2294.
29. Wilham JM, Orru CD, Bessen RA, Atarashi R, Sano K, Race B, Meade-White KD, Taubner LM, Timmes A, Caughey B. 2010. Rapid end-point quantitation of prion seeding activity with sensitivity comparable to bioassays. PLoS Pathog. 6:e1001217. http://dx.doi.org/10.1371/journal.ppat.1001217.
30. Atarashi R, Moore RA, Sim VL, Hughson AG, Dorward DW, Onwubiko HA, Priola SA, Caughey B. 2007. Ultrasensitive detection of scrapie prion protein using seeded conversion of recombinant prion protein. Nat. Methods 4:645–650. http://dx.doi.org/10.1038/nmeth1066.
31. Fujihara A, Atarashi R, Fuse T, Ubagai K, Nakagaki T, Yamaguchi N, Ishibashi D, Katamine S, Nishida N. 2009. Hyperefficient PrP Sc amplification of mouse-adapted BSE and scrapie strain by protein misfolding cyclic amplification technique. FEBS J. 276:2841–2848. http://dx.doi.org/10.1111/j.1742-4658.2009.07007.x.
32. Kocisko DA, Lansbury PT, Jr, Caughey B. 1996. Partial unfolding and refolding of scrapie-associated prion protein: evidence for a critical 16-kDa C-terminal domain. Biochemistry 35:13434–13442. http://dx.doi.org/10.1021/bi9610562.
33. Atarashi R, Sano K, Satoh K, Nishida N. 2011. Real-time quaking-induced conversion: a highly sensitive assay for prion detection. Prion 5:150–153. http://dx.doi.org/10.4161/pri.5.3.16893.
34. Smirnovas V, Baron GS, Offerdahl DK, Raymond GJ, Caughey B, Surewicz WK. 2011. Structural organization of brain-derived mammalian prions examined by hydrogen-deuterium exchange. Nat. Struct. Mol. Biol. 18:504–506. http://dx.doi.org/10.1038/nsmb.2035.
35. McGuire LI, Peden AH, Orru CD, Wilham JM, Appleford NE, Mallinson G, Andrews M, Head MW, Caughey B, Will RG, Knight RS, Green AJ. 2012. Real time quaking-induced conversion analysis of cerebrospinal fluid in sporadic Creutzfeldt-Jakob disease. Ann. Neurol. 72:278–285. http://dx.doi.org/10.1002/ana.23589.
36. Orru CD, Wilham JM, Raymond LD, Kuhn F, Schroeder B, Raeber AJ, Caughey B. 2011. Prion disease blood test using immunoprecipitation and improved quaking-induced conversion. mBio 2(3):e00078-00011. http://dx.doi.org/10.1128/mBio.00078-11.
37. Sano K, Satoh K, Atarashi R, Takashima H, Iwasaki Y, Yoshida M, Sanjo N, Murai H, Mizusawa H, Schmitz M, Zerr I, Kim YS, Nishida N.

2013. Early detection of abnormal prion protein in genetic human prion diseases now possible using real-time QUIC assay. PLoS One 8:e54915. http://dx.doi.org/10.1371/journal.pone.0054915.
38. Vascellari S, Orru CD, Hughson AG, King D, Barron R, Wilham JM, Baron GS, Race B, Pani A, Caughey B. 2012. Prion seeding activities of mouse scrapie strains with divergent PrPSc protease sensitivities and amyloid plaque content using RT-QuIC and eQuIC. PLoS One 7:e48969. http://dx.doi.org/10.1371/journal.pone.0048969.
39. Henderson DM, Manca M, Haley NJ, Denkers ND, Nalls AV, Mathiason CK, Caughey B, Hoover EA. 2013. Rapid antemortem detection of CWD prions in deer saliva. PLoS One 8:e74377. http://dx.doi.org/10.1371/journal.pone.0074377.
40. Smirnovas V, Kim JI, Lu X, Atarashi R, Caughey B, Surewicz WK. 2009. Distinct structures of scrapie prion protein (PrPSc)-seeded versus spontaneous recombinant prion protein fibrils revealed by hydrogen/deuterium exchange. J. Biol. Chem. 284:24233–24241. http://dx.doi.org/10.1074/jbc.M109.036558.
41. Hornemann S, Schorn C, Wuthrich K. 2004. NMR structure of the bovine prion protein isolated from healthy calf brains. EMBO Rep. 5:1159–1164. http://dx.doi.org/10.1038/sj.embor.7400297.
42. Clarke AR, Jackson GS, Collinge J. 2001. The molecular biology of prion propagation. Philos. Trans. R. Soc. Lond. B Biol. Sci. 356:185–195. http://dx.doi.org/10.1098/rstb.2000.0764.
43. Lawson VA, Collins SJ, Masters CL, Hill AF. 2005. Prion protein glycosylation. J. Neurochem. 93:793–801. http://dx.doi.org/10.1111/j.1471-4159.2005.03104.x.
44. Aguzzi A, Heikenwalder M, Polymenidou M. 2007. Insights into prion strains and neurotoxicity. Nat. Rev. Mol. Cell Biol. 8:552–561. http://dx.doi.org/10.1038/nrm2204.
45. Cancellotti E, Mahal SP, Somerville R, Diack A, Brown D, Piccardo P, Weissmann C, Manson JC. 2013. Post-translational changes to PrP alter transmissible spongiform encephalopathy strain properties. EMBO J. 32:756–769. http://dx.doi.org/10.1038/emboj.2013.6.
46. Piro JR, Harris BT, Nishina K, Soto C, Morales R, Rees JR, Supattapone S. 2009. Prion protein glycosylation is not required for strain-specific neurotropism. J. Virol. 83:5321–5328. http://dx.doi.org/10.1128/JVI.02502-08.
47. Mahal SP, Jablonski J, Suponitsky-Kroyter I, Oelschlegel AM, Herva ME, Oldstone M, Weissmann C. 2012. Propagation of RML prions in mice expressing PrP devoid of GPI anchor leads to formation of a novel, stable prion strain. PLoS Pathog. 8:e1002746. http://dx.doi.org/10.1371/journal.ppat.1002746.
48. Li J, Browning S, Mahal SP, Oelschlegel AM, Weissmann C. 2010. Darwinian evolution of prions in cell culture. Science 327:869–872. http://dx.doi.org/10.1126/science.1183218.
49. Weissmann C, Li J, Mahal SP, Browning S. 2011. Prions on the move. EMBO Rep. 12:1109–1117. http://dx.doi.org/10.1038/embor.2011.192.
50. Shikiya RA, Ayers JI, Schutt CR, Kincaid AE, Bartz JC. 2010. Coinfecting prion strains compete for a limiting cellular resource. J. Virol. 84:5706–5714. http://dx.doi.org/10.1128/JVI.00243-10.
51. Bieschke J, Weber P, Sarafoff N, Beekes M, Giese A, Kretzschmar H. 2004. Autocatalytic self-propagation of misfolded prion protein. Proc. Natl. Acad. Sci. U. S. A. 101:12207–12211. http://dx.doi.org/10.1073/pnas.0404650101.
52. Klingeborn M, Race B, Meade-White KD, Chesebro B. 2011. Lower specific infectivity of protease-resistant prion protein generated in cell-free reactions. Proc. Natl. Acad. Sci. U. S. A. 108:E1244–E1253. http://dx.doi.org/10.1073/pnas.1111255108.
53. Gonzalez-Montalban N, Lee YJ, Makarava N, Savtchenko R, Baskakov IV. 2013. Changes in prion replication environment cause prion strain mutation. FASEB J. 27:3702–3710. http://dx.doi.org/10.1096/fj.13-230466.

Journal of General Virology (2014), **95**, 2576–2588 DOI 10.1099/vir.0.066225-0

Ultrasensitive detection of PrP^{Sc} in the cerebrospinal fluid and blood of macaques infected with bovine spongiform encephalopathy prion

Yuichi Murayama,[1] Kentaro Masujin,[1] Morikazu Imamura,[1] Fumiko Ono,[2] Hiroaki Shibata,[3] Minoru Tobiume,[4] Tomoaki Yamamura,[1] Noriko Shimozaki,[1] Keiji Terao,[3] Yoshio Yamakawa[5] and Tetsutaro Sata[4]

Correspondence
Yuichi Murayama
ymura@affrc.go.jp

[1]Influenza and Prion Disease Research Center, National Institute of Animal Health, Tsukuba, Ibaraki, Japan

[2]Chiba Institute of Science Faculty of Risk and Crisis Management, Choshi, Chiba, Japan

[3]Tsukuba Primate Research Center, National Institute of Biomedical Innovation, Tsukuba, Ibaraki, Japan

[4]Department of Pathology, National Institute of Infectious Diseases, Tokyo, Japan

[5]Department of Biochemistry and Cell Biology, National Institute of Infectious Diseases, Tokyo, Japan

Prion diseases are characterized by the prominent accumulation of the misfolded form of a normal cellular protein (PrP^{Sc}) in the central nervous system. The pathological features and biochemical properties of PrP^{Sc} in macaque monkeys infected with the bovine spongiform encephalopathy (BSE) prion have been found to be similar to those of human subjects with variant Creutzfeldt–Jakob disease (vCJD). Non-human primate models are thus ideally suited for performing valid diagnostic tests and determining the efficacy of potential therapeutic agents. In the current study, we developed a highly efficient method for *in vitro* amplification of cynomolgus macaque BSE PrP^{Sc}. This method involves amplifying PrP^{Sc} by protein misfolding cyclic amplification (PMCA) using mouse brain homogenate as a PrP^{C} substrate in the presence of sulfated dextran compounds. This method is capable of amplifying very small amounts of PrP^{Sc} contained in the cerebrospinal fluid (CSF) and white blood cells (WBCs), as well as in the peripheral tissues of macaques that have been intracerebrally inoculated with the BSE prion. After clinical signs of the disease appeared in three macaques, we detected PrP^{Sc} in the CSF by serial PMCA, and the CSF levels of PrP^{Sc} tended to increase with disease progression. In addition, PrP^{Sc} was detectable in WBCs at the clinical phases of the disease in two of the three macaques. Thus, our highly sensitive, novel method may be useful for furthering the understanding of the tissue distribution of PrP^{Sc} in non-human primate models of CJD.

Received 24 March 2014
Accepted 10 July 2014

INTRODUCTION

Transmissible spongiform encephalopathies (TSEs), commonly known as prion diseases, are fatal neurodegenerative disorders that affect both animals and humans (Collinge, 2001). Prion diseases are characterized by the prominent accumulation of a misfolded prion protein, PrP^{Sc}, in the central nervous system (Prusiner, 1991, 1998). PrP^{Sc}, which is rich in beta-sheet structures and resistant to digestion by proteases and various inactivating treatments (Caughey *et al.*, 1991; Pan *et al.*, 1993), is considered to be the infectious agent for TSEs and appears to self-propagate through post-translational modification of the normal prion protein PrP^{C} (Prusiner, 1998).

One type of human prion disease, Creutzfeldt–Jakob disease (CJD), can be aetiologically identified as sporadic, inherited or acquired by infection (Ironside, 1998; Belay, 1999; Glatzel *et al.*, 2002; Geissen *et al.*, 2007). In variant CJD (vCJD), which is a form of CJD caused by consumption of foods contaminated with bovine spongiform encephalopathy (BSE) prions (Will *et al.*, 1996; Hill *et al.*, 1997; Ironside, 2010), small amounts of PrP^{Sc} have been found in a broad range of peripheral tissues, including the lymph nodes, tonsils, spleen, kidneys, portions of the intestinal tract and skeletal muscle (Wadsworth *et al.*, 2001; Hilton *et al.*, 2004; Peden *et al.*, 2006; Notari *et al.*, 2010), as well as in the

Four figures and one table are available with the online version of this paper.